DHX30 coordinates cytoplasmic translation and mitochondrial function contributing to cancer cell survival

Bartolomeo Bosco[1], Annalisa Rossi[1], Dario Rizzotto[1^], Sebastiano Giorgetta[1], Alicia Perzolli[1], Francesco Bonollo[1], Angeline Gaucherot[2], Frédéric Catez[2], Jean-Jacques Diaz[2], Erik Dassi[1#], Alberto Inga[1#]

[1]Department of Cellular, Computational and Integrative Biology, CIBIO, University of Trento, via Sommarive 9, 38123, Trento, Italy

[2]Inserm U1052, CNRS UMR5286 Centre de Recherche en Cancérologie de Lyon, F-69000 Lyon, France. Centre Léon Bérard, F-69008 Lyon, France, Université de Lyon 1, F-69000 Lyon, France

^present address: CeMM Research Center for Molecular Medicine of the Austrian Academy of Sciences, Vienna, Austria

#corresponding authors:
erik.dassi@unitn.it
alberto.inga@unitn.it

Running title: DHX30 controls global translation

Keywords: DHX30, translation efficiency, polysomal profiling, mitoribosome, ribosome biogenesis, RNA binding proteins

Abstract

DHX30 was recently implicated in the translation control of mRNAs involved in p53-dependent apoptosis. Here we show that DHX30 exhibits a more general function by integrating the activities of its cytoplasmic isoform and of the more abundant mitochondrial one. The depletion of both DHX30 isoforms in HCT116 cells leads to constitutive changes in polysome-associated mRNAs, enhancing the translation of mRNAs coding for cytoplasmic ribosomal proteins while reducing the translational efficiency of the nuclear-encoded mitoribosome mRNAs. Furthermore, depletion of both DHX30 isoforms exhibits higher global translation but slower proliferation, and reduced mitochondrial energy metabolism. Isoform-specific silencing established a role for cytoplasmic DHX30 in modulating global translation. The impact on global translation and proliferation were confirmed in U2OS and MCF7 cells, although the effect of DHX30 depletion on mitochondrial gene expression was observed only in MCF7 cells. Exploiting RIP, eCLIP, and gene expression data, we identified a gene signature comprising DHX30 and fourteen mitoribosome transcripts that we candidate as direct targets: this signature shows prognostic value in several TCGA cancer types, with higher expression associated with reduced overall survival. We propose that DHX30 contributes to cell homeostasis by coordinating ribosome biogenesis, global translation, and mitochondrial metabolism. Targeting DHX30 could, thus, expose a vulnerability in cancer cells.

Author summary

Translation occurs in the cell both through cytoplasmic and mitochondrial ribosomes, respectively translating mRNAs encoded by the nuclear and the mitochondrial genome. Here we found that DHX30, an RNA-binding protein implicated in p53-dependent apoptosis, enhances the translation of mRNAs coding for cytoplasmic ribosomal proteins while reducing that of the mitoribosome mRNAs when silenced. This coordination of the cytoplasmic and mitochondrial translation machineries affected both cell proliferation and energy metabolism, suggesting an important role for this mechanism in determining the fitness of cancer cells. Indeed, the analysis of publicly available cancer datasets led us to define a 15-genes signature that is able to affect the prognosis of a subset of cancer types. In this subset, we found that higher expression of the genes composing

67 the signature is associated with a worse prognosis. We thus propose DHX30 as a potential
68 vulnerability in cancer cells, that could be targeted to develop novel therapeutic strategies.
69
70
71 **Introduction**
72 The DHX30 RNA binding protein (RBP) is an ATP-dependent RNA helicase highly expressed in neural
73 cells and somites during embryogenesis in mice. It plays an important role in development and its
74 homozygous deletion is lethal for embryos [1]. In humans, DHX30 is involved in the antiviral function of
75 the zinc-finger ZAP protein. Indeed, it was demonstrated that these two proteins directly interact with each
76 other via the N-terminal domain and that DHX30 is necessary for the optimal antiviral activity of ZAP [2].
77 Recently, six de novo missense mutations were identified in DHX30 in twelve unrelated patients affected
78 by global developmental delay (GDD), intellectual disability (ID), severe speech impairment and gait
79 abnormalities [3]. All mutations caused amino acid changes in the highly conserved helicase motif,
80 impairing the protein's ATPase activity or RNA recognition. Moreover, overexpression of those DHX30
81 mutants led to increased propensity to trigger stress granules (SG) formation and decreased global
82 translation [3]. It was shown that DHX30 could play an important role also in human fibroblast and
83 osteosarcoma mitochondria. Indeed, in that compartment it interacts with a Fas-activated serine-threonine
84 kinase (FASTKD2), modulating mitochondrial ribosome maturation and assembly [4].
85 Our group and collaborators recently compared p53-mediated responses to Nutlin-3 treatment in three
86 different cancer cell lines: HCT116, SJSA1 and MCF7 [5,6]. It was observed that p53 activation caused
87 cell cycle arrest in HCT116, massive apoptosis in SJSA1 and an intermediate phenotype in MCF7,
88 consistent with earlier reports [7]. By analyzing the cell lines' translatomes (i.e. transcripts loaded on
89 polysomes and in active translation), we discovered that only 0.2% of the genes were commonly
90 differentially expressed (DEGs). Furthermore, the polysome profiling of SJSA1 revealed an enrichment
91 of pro-apoptotic transcripts [6] in the fraction corresponding to polysomes. Those featured instances of a
92 specific cis-element in their 3'UTR, labeled as CGPD, standing for CG-rich motif for p53-dependent death.
93 The DExH box RNA helicase DHX30 was found to be one RBP whose binding to the CGPD motif
94 correlated with a specific cell fate. Indeed, DHX30 was expressed at higher levels in HCT116 than SJSA1,

95 resulting in a lower translation of GCPD-motif-containing transcripts in HCT116 cells. Depletion of
96 DHX30 in HCT116 by stable shRNA increased the translation potential of mRNAs containing the CGPD
97 motif, resulting in higher levels of apoptosis after p53 activation by Nutlin treatment, mimicking in part the
98 apoptotic phenotype of SJSA1 [6].
99 In this work, we set to determine the broader phenotypic role of DHX30 in the colorectal cancer cell line
100 HCT116. By virtue of two alternative promoters leading to the production isoforms containing or not a
101 mitochondrial localization signal, DHX30 can couple mitochondrial function, ribosome biogenesis and
102 global translation. Depleting DHX30 in HCT116 cells reduced cell proliferation and sensitised cells to
103 small molecules targeting mitochondrial function. Results were extended to two different cancer cell
104 models and their implications explored using TGCA data.
105
106 **Results**
107 *DHX30 depletion enhances translation in HCT116 cells*
108 We previously identified DHX30 as a negative modulator of p53-dependent apoptosis, performing
109 polysomal profiling followed by RNA-seq of HCT116 cells clones stably depleted for DHX30 and treated
110 with the MDM2 inhibitor Nutlin-3 [7]. Here we reanalyzed this dataset (GSE95024), complementing it by
111 performing a total-cytoplasmic RNA profiling of the same cells by RNA-seq (GSE154065), and focusing
112 on the comparison between DHX30-depleted (shDHX30) and control (shNT) HCT116 cells in the untreated
113 control.
114 We compared the gene expression changes at the polysomal or total cytoplasmic RNA levels and
115 performed a gene set enrichment analysis [8]. This revealed an increased abundance of ribosomal proteins
116 and ribosome biogenesis genes in shDHX30 cells, only at the polysomal level (**Figure 1A**, **Table S1**).
117 Consistently, analysis of translation efficiency (TE), measured as the ratio between relative RNA abundance
118 in polysomal and total cytoplasmic fractions, revealed that DHX30 depletion is associated with higher TE
119 for transcripts coding for ribosomal protein subunits (RPL, RPS, **Figure 1B**). On the other end, nuclear
120 transcripts coding mitochondrial ribosomal proteins exhibited reduced TE in DHX30-depleted cells, despite
121 showing higher constitutive TE compared to the cytoplasmic ribosomal transcripts (mRPL, mRPS, **Figure**
122 **1B**). Validation by qPCR was performed for four RPs and four MRPs transcripts (**Figure S1A**). The basal

123 differences in TE between ribosome and mitoribosome transcripts was confirmed in all cases, and for five
124 of them results reproduced the effect of DHX30 depletion on TE that was observed from the RNA-seq data.
125 A trend for higher expression of RPL and RPS transcripts and lower expression of MRPL and MRPS
126 transcripts in DHX30-depleted cells was also apparent (**Figure S1B**).
127 We thus sought to understand if DHX30 could be directly regulating this class of genes and exploited the
128 data of DHX30 eCLIP assay performed in K562 cells as part of the ENCODE project [9]. Despite the
129 different cell line, the eCLIP data indicate that DHX30 can bind 67 ribosomal (36 RPLs and 31 RPSs) and
130 23 mitoribosomal (16 MRPLs and 7 MRPSs) protein transcripts (**Table S1**) [9].
131 Consistent with the higher TE for RPL and RPS transcripts, DHX30 depletion in HCT116 cells
132 was associated with higher relative amounts of ribosomes extracted and quantified from a sucrose cushion
133 (**Figure 1C**), and higher rRNA levels (**Figure 1D, E**). Furthermore, DHX30-depleted cells not only showed
134 evidence of increased ribosome biogenesis, but also of higher global translation (**Figure 1F, 1G**). The
135 higher global translation does not appear to be related to an increase in MYC expression or activity (**Figure**
136 **S1C**), nor to a significant increase in the activity mTOR pathway (**Figure S1D**). Finally, DHX30 protein
137 was found to be associated with ribosomal subunits, 80S monosomes as well as with low molecular-weight
138 polysomes in HCT116, MCF7 and U2OS cells (**Figure S1F**).
139 Hence, DHX30 appears to negatively influence ribosome biogenesis, global translation and also
140 the translation of specific mRNAs. It is important to emphasize that these are not necessarily dissociated
141 events, as a change in ribosome number could be sufficient to impact on translation specificity [10].
142
143 *DHX30 depletion alters the expression of mitoribosomal transcripts*
144 The impact of DHX30 depletion on the expression and translation efficiency of nuclear-encoded
145 mitoribosomal proteins caught our attention, as it showed the opposite trend compared to ribosomal protein
146 transcripts (**Figure 1B, Figure S1**). First, we established the potential for DHX30 to bind to mitoribosomal
147 protein transcripts by RIP assays, choosing MRPL11 (UL11m), that was previously evaluated in cancer
148 cells [3], and MRPS22 (mS22), as a representative of the large and small subunits, respectively (**Figure**
149 **2A**). Next, we observed that DHX30-depleted cells showed reduced expression of these two genes at both
150 the RNA and protein levels (**Figure 2B, C**). These findings suggest that DHX30 directly promotes stability

151 and/or translation of mitoribosome transcripts. The modulation of mitoribosome proteins expression might
152 impact on mitochondrial translation and contribute to the functions described for DHX30 in the
153 mitochondrial matrix [4,11]. Notably, the DHX30 gene contains two promoters, and the transcript resulting
154 from the internal, more 3'- one (ENST00000457607.1) includes an alternative first exon that contains a
155 predicted mitochondrial targeting sequence [12,13]. Mitochondrial localization of the protein was
156 confirmed by immunofluorescence (**Figure 2D**), consistent with previous results in human fibroblasts [4]
157 and APEX-seq data [14]. We checked the relative levels of the DHX30 transcripts from the two promoters
158 and found the putative mitochondrial isoform to be about four times more abundant (**Figure 2E**), as
159 indicated also by western blot analysis on extracts of mitochondrial and cytoplasmic fractions (**Figure 2F**).
160 Stable DHX30-silencing was obtained using three different shRNAs [6] that targeted both
161 cytoplasmic and mitochondrial transcripts (from here on labeled cDHX30 and mDHX30) (**Figure S2A**),
162 and isolating single clones. To confirm results, we also employed transient silencing using one siRNA
163 specific for cDHX30 (labeled siDHX30-C) or an siRNA targeting transcripts from both promoters (labeled
164 siDHX30-C+M). The activity and specificity of the two siRNAs was assessed by qRT-PCR 48 and 96 hours
165 post-silencing (**Figure S2B**, **Figure 3A**). Transient silencing of just cDHX30 or both cDHX30 and
166 mDHX30 for 96 hours led to an increase in global translation (**Figure 3B**) that was not associated with an
167 increase in the activity mTOR pathway (**Figure S1E**), thus confirming the observations obtained with the
168 different stable clones, but indicating that cDHX30 modulates global translation.
169 Transient silencing of both cDHX30 and mDHX30 resulted in a reduction of the expression of
170 MRPL11 and MRPS22 (**Figure 3C, D**) similar to what we previously observed with stable depletion of
171 both isoforms (Figure 2), while cDHX30 silencing was ineffective, considering the results at both RNA and
172 protein levels.
173 DHX30 stable or transient silencing was extended to U2OS, osteosarcoma-derived cells that
174 express relatively high levels of DHX30 (**Figure S2C, S2D**). Stable depletion of both cDHX30 and
175 mDHX30 was associated with a significant reduction of MRPL11 (RNA and protein) and of MRPS22
176 mRNA expression (**Figure S2E, S2F**), while transient depletion by siRNAs did not significantly impact on
177 the expression of the two mitoribosome transcripts (**Figure S2G**), although MRPL11 protein levels were
178 reduced by siDHX30-C+M (**Figure S2H**).

179 Transient silencing of both cDHX30 and mDHX30 was also performed in the breast cancer-derived
180 MCF7 cells (**Figure S3A**) and led to a reduction in the expression of both MRPL11 and MRPS22 mRNAs
181 (**Figure S3B**), although only for MRPL11 the effect was consistent also at protein level (**Figure S3C**).
182 Cytoplasmic DHX30 transient silencing in U2OS and MCF7 also led to higher global translation,
183 confirming the results obtained in HCT116 cells (**Figure S3D**, **S3E**).
184
185 *DHX30 depletion impacts mitochondrial gene expression and function*
186 We next focused on the expression of mitochondrially encoded genes. First of all, we established
187 that DHX30 depletion did not impact on the number of mitochondrial genomes by digital PCR in HCT116
188 cells (**Figure 4A**). Instead, the expression of several mitochondrially encoded transcripts was significanly
189 reduced (**Figure 4B**). The steady-state expression of two mitochondrially encoded proteins, MT-ATP6 and
190 MT-ATP8, was investigated and shown to be reduced in HCT116_shDHX30 cells (**Figure 4C, S3F**). We
191 pursued the same analysis after transient silencing, confirming the lower expression of mitochondrially
192 encoded genes at the RNA and protein levels, but only when the DHX30 mitochondrial variant (siDHX30-
193 C+M) was silenced and analysed 96 hours post silencing (**Figure 4D, 4E**). In fact, although DHX30
194 depletion was visible already after 48 hours (**Figure S2B**) from the addition of the siRNAs, more time was
195 needed to appreciate a reduction in the expression of mitochondrially encoded genes. The expression of
196 mitochondrially encoded genes was checked also after DHX30 silencing in U2OS and MCF7 cells (**Figure**
197 **S4**). In U2OS_shDHX30 cells, all of the tested transcripts, with the exception of MT-ND6, were down-
198 modulated compared to the U2OS_shNT control (**Figure S4A,** left panel). Instead, none of the seven tested
199 transcripts were down-modulated by transient DHX30 silencing, regardless of the siRNA used (**Figure**
200 **S4A,** right panel). In fact, three of them were slightly upregulated. This latter result is consistent with the
201 observation of a slightly lower efficacy of DHX30 depletion by siRNAs and with the lack of an impact on
202 MRPL11 or MRPS22 expression (Figure S2). MT-ATP6 was also examined by western blot and its amount
203 was reduced in U2OS_shDHX30 cells (**Figure S4C**), but not in U2OS cells that were transiently silenced
204 for DHX30 (**Figure S4D**). Transient DHX30 depletion (by siDHX30 C+M) in MCF7 cells led to a
205 significant reduction in the expression of all tested mitochondrial transcripts, although for MT-ATP6 the
206 reduction was not significant at protein levels (**Figure S4B, S4E**).

207 Finally, we evaluated markers of carbon metabolism and mitochondrial respiration capacity by an
208 Agilent SeahorseXF real-time analyzer. HCT116_shDHX30 cells had a significantly lower basal oxygen
209 consumption rate compared to the control cell line. Notably, DHX30-depleted cells did not show
210 compensatory glycolysis in basal culture condition, not even when we chemically abolished mitochondrial
211 respiration. We indeed observed a lower compensatory glycolysis compared with the control (**Figure 4F**).
212 These results suggest that HCT116_shDHX30 cells do not show a typical Warburg effect [15], and are
213 expected to produce less energy due to reduced mitochondrial respiration.
214 Collectively, the depletion of DHX30 seems to generate an imbalance in cell homeostasis, with higher
215 demand of chemical energy from ribosome biogenesis and cytoplasmic translation but lower mitochondrial
216 activity.
217
218 *DHX30 depletion impaired cell proliferation rate and increased apoptosis proneness.*
219 Next, we characterized the phenotypic impact of DHX30 depletion in HCT116. Consistent with the lower
220 mitochondrial oxygen consumption rate, HCT116_shDHX30 cells showed a significantly lower
221 proliferation rate compared to the control cell clone. This was observed by colony formation assay and
222 confirmed through time-course proliferation by cell count via high-content microscopy or using a Real-
223 Time Cell Analyzer xCELLigence (**Figure 5A-C**). Interestingly, we observed a reduction in proliferation
224 after DHX30 silencing also in a spheroid assay (**Figure 5D**). The lower growth rate in DHX30 depleted
225 cells cannot be attributed to an arrest in a particular phase of the cell cycle (**Figure 5E**). Instead, it could be
226 associated with a moderate increase in the phosphorylation of eIF2alpha (**Figure 5F**), but not to an obvious
227 ER-stress response, based on the expression of CHOP, DDIT4, TRIB3, and on the XBP1 splicing pattern
228 (**Figure S5A**).
229 A reduction in proliferation was confirmed also by cell counting upon transient silencing of cDHX30 and,
230 particularly, of both cDHX30 and mDHX30 (**Figure 5G**). The impact on cell proliferation was also
231 examined using U2OS cells stably depleted for DHX30 that showed a significant reduction of proliferation
232 compared to the U2OS_shNT control (**Figure S5B**). Transient silencing did not impact on the proliferation
233 of U2OS cells, consistent with the results observed on DHX30 target gene expression, while it led to a
234 significant reduction in MCF7 cells (**Figure S5B**).

235 Furthermore, DHX30 depletion was associated with increased apoptosis after 48 hours of Nutlin
236 treatment, as expected by our previous results [6], but also when cells were treated with the topoisomerase
237 inhibitor doxorubicin and with FCCP, an agent that causes mitochondrial membrane depolarization (**Figure**
238 **5H**).
239
240 *DHX30 signature and cancer outcome*
241 Our results suggest that DHX30 exerts a constitutive function that improves cellular fitness by balancing
242 energy metabolism and global translation potential. Furthermore, our previous study identified DHX30 as
243 a negative modulator of the translation of specific mRNAs, thus controlling p53-dependent apoptosis [6].
244 Both these functions suggest that DHX30 could be a modifier of cancer cell properties potentially impacting
245 on clinical variables.
246 Although total RNA-seq data are not a good proxy for investigating translation controls [16], in
247 this study we showed that DHX30 depletion impacts on steady-state levels of nuclear-encoded
248 mitoribosomal transcripts. MRPL11 and, particularly, MRPS22 can be considered direct DHX30 targets.
249 We next cross-referenced our TE and GSEA data with the RIP results and DHX30 eCLIP data in ENCODE
250 [9] and compiled a list of 14 mitoribosomal protein (MRP) transcripts considered DHX30 direct target
251 candidates (**Figure 6**, **Figure S6**). Interrogating RNA-seq data of TGCA tumors through the GEPIA web
252 resource [17,18], the expression of DHX30, and of each MRP transcript or of the group of 14 candidate
253 target MRPs appeared to be positively correlated in several cancer types (**Figure 6, Figure S6**), including
254 adrenocortical carcinoma, and hepatocellular carcinomas. No such correlation was instead apparent for
255 other cancer types, including breast or colon adenocarcinomas. We next used this gene signature to stratify
256 patients' clinical outcome. Interestingly, for the cancer types where a positive correlation in the expression
257 of DHX30 and the 14 MRPs was observed, the combined 15-gene signature (*i.e.* including DHX30) showed
258 a prognostic value. In particular, higher expression was associated with reduced Overall Survival or
259 Disease-Free Survival (**Figure 6**). Instead, the comparison of DHX30 expression between tumors and
260 matched controls did not show a consistent trend but confirmed a rather wide variation among samples, and
261 tissue-specific effects including both cases of over-expression and down-regulation (**Figure S7**). Finally, a
262 pan-tissue view revealed a general positive correlation between the expression of ribosome and

263 mitoribosome protein transcripts in normal samples, that is lost in cancer (**Figure S8**). These preliminary
264 analyses suggest that a functional signature could be developed to predict aggressiveness in cancer types
265 where DHX30 appears to stimulate mitoribosomal proteins expression.
266
267 **Discussion**
268 Ribosome biogenesis and translation impose a high metabolic demand on the cell [19,20]. Hence, a
269 coordination between translational control and metabolic output ultimately involving mitochondrial
270 respiratory functions is expected to contribute to cell homeostasis and fitness [21,22]. However, relatively
271 few proteins and pathways have been established to exert a direct role in balancing cytoplasmic translation
272 initiation with mitochondrial metabolism [23,24]. eIF6 represents a significant example, as it has been
273 clearly shown that it negatively controls 80S monosome assembly, a necessary step for translation initiation,
274 while at the same time playing a critical positive role in mitochondrial functions, as revealed by broad
275 changes in the mitochondrial proteome in eIF6 hemizygous mice [25–27].
276 We propose that DHX30 can also exert an important housekeeping role in coordinating ribosome
277 biogenesis, translation, and mitochondrial respiration. DHX30 depletion in HCT116, stable or transient,
278 leads to a modest but significant increase in ribosome biogenesis as well as in global translation; on the
279 contrary, mito-ribosome transcripts, particularly of the large subunits, exhibit reduced translation
280 efficiency. Furthermore, DHX30 can also exert a more direct role on mitochondria, as the protein can
281 directly localize to the organelle, thanks to an alternative first exon that features a localization signal. The
282 steady state expression of several mitochondrially encoded genes was reduced following the depletion of
283 both DHX30 transcripts and perhaps more effectively, by the reduction of the mitochondrial isoform. A
284 previous study provided clear evidence that DHX30 together with DDX28, FASTKD2, and FASTKD5 can
285 promote the assembly of 55S mito-monosome and translation [4]. Consistent with the relevance of a
286 mitochondrial and translation function, the DHX30 transcript has been shown to be located and locally
287 translated at the ER-Outer Mitochondrial membrane interface, by APEX-seq [14]. In fact, none of the
288 DHX30 closer homologs showed strong evidence of such localized translation, or other evidence of
289 mitochondrial localization.

290 A previous report also showed evidence for DHX30 interaction with mitochondrial transcripts in
291 human fibroblasts by RIP-seq [4]. Our data instead point to a direct interaction with mitoribosome
292 transcripts and their positive modulation as another means by which DHX30 can indirectly affect
293 mitochondrial translation. We validated by RIP the binding of DHX30 to MRPL11 and MRPS22.
294 Leveraging public data from eCLIP experiments in ENCODE and our polysomal profiling, RNA-seq, and
295 GSEA analysis, we propose that DHX30 could directly interact with fourteen mito-ribosome protein
296 transcripts. An even larger set of ribosomal protein transcripts are nominated as direct DHX30 targets by
297 eCLIP [9] and are showing changes in translation efficiency upon DHX30 depletion in HCT116 cells.
298 We observed that these two groupings of transcripts markedly differed for their basal translation
299 efficiency, which was low for cytoplasmic ribosomal protein transcripts. Those mRNAs are known to
300 contain particularly structured 5'-UTR and to be strongly regulated at the level of translation initiation by
301 mTOR and MYC-regulated pathways [28–30]. The mechanism by which DHX30 can control ribosomal
302 protein (RP) transcripts remains to be established. In a recent study, we discovered an RNA sequence motif
303 in 3'UTRs, labeled CGPD, that is targeted by DHX30 and can mediate higher translation levels [6]. While
304 we cannot exclude that the CGPD motif could be implicated, only a subset of RP transcripts harbors
305 instances of it. Our *de novo* search for over-represented motifs did not retrieve another prominent candidate
306 *cis*-element. An even lower number of mito-RP transcripts were found to harbor instances of the CGPD-
307 motif. This was expected, as DHX30 is inferred to have an opposite role on RP and mito-RP transcripts
308 based on the direction of changes in their TE observed in HCT116 shDHX30 cells. For the mito-RP gene
309 group, a *de novo* motif over-representation search did not identify a strongly enriched cis-element.
310 The magnitude of fold-change and translation efficiency changes for both ribosomal and
311 mitoribosomal transcripts in response to DHX30 silencing is modest in absolute value. This could be in
312 part due to a limitation of the experimental approach. As reported in our earlier study, a complete knock-
313 out of DHX30 does not seem to be attainable in HCT116 cells. Both our siRNA and even more so the
314 shRNA clones retain partial DHX30 expression. Furthermore, it is important to emphasize that changes in
315 the expression or even polysomal association of ribosomal protein transcripts do not necessarily predict
316 translation rate changes. However, several endpoints consistently suggested that HCT116 shDHX30 cells
317 exhibited higher ribosome number and increased global translation. When treated with an MDM2 inhibitor

318 inducing strong p53-dependent transcriptional response, those cells were also shown to markedly alter their
319 translatome [6]. Our results pointed to a direct role of DHX30 on translation specificity. However, we
320 cannot exclude that the global effect on ribosome biogenesis we propose represents a constitutive,
321 housekeeping function for DHX30. This function would also contribute to the observed changes in
322 translation specificity, under the notion that a change in global translation potential or in the modulation of
323 translation initiation is not expected to impact equally every available transcript in a cell [10,22].

324 Depletion of DHX30 reduced cell proliferation in various assays. This effect was visible also by
325 transient silencing of just the cytoplasmic transcript, although it was more evident when both cytoplasmic
326 and mitochondrial isoforms were targeted. Although we cannot exclude that the lower proliferation results
327 from a checkpoint activation, as we have seen that in the siRNA experiments the lack of p53 can reduce the
328 proliferation lag (**Figure S9**), cells did not show evidence for overt cell cycle arrest. This is not entirely
329 unexpected, due to the residual levels of DHX30 expression in the cell models we used, as noted above,
330 and also for the possible selective pressure for compensatory effects given the central nature of the processes
331 involved. Transient silencing of DHX30 in HCT116 p53 null cells besides having a reduced impact on
332 proliferation also did not significantly alter the expression of MRPS22, MRPL11 or of mitochondrial
333 transcripts. While this may be suggestive of a functional interaction between DHX30 and p53, results may
334 be affected by the lower efficiency of DHX30 depletion in HCT116 $p53^{-/-}$ cells (**Figure S9**).

335 As several other RBPs, mito-ribosomal proteins have been proposed to have additional,
336 moonlighting functions unrelated to mito-ribosome biogenesis, in particular in the modulation of apoptosis.
337 For example, MRPS29, also known as DAP3, was reported to influence the extrinsic apoptosis pathway
338 [31,32], while MRPL41 was proposed to modulate p53-dependent intrinsic apoptosis [33]. It is, however,
339 unlikely that these potential pro-apoptotic functions can contribute to the proliferation defects seen after
340 DHX30 depletion, given that their expression is not significantly modified. The expression of several mito-
341 ribosome components has been evaluated as potential biomarkers associated with cancer clinical variables
342 [34].

343 Hence, we reasoned that changes in DHX30 levels to an extent that would not lead to overt stress
344 responses could provide opportunities for increased fitness due to the coordination between mitochondrial
345 function and translation potential, which could be a balancing function between energy supply and demand.

346 If any, the effects would be expected to reflect tissue-specific differences in metabolism. We explored
347 TGCA data, first evaluating if a positive correlation could be observed in normal tissue and/or primary
348 cancer samples for DHX30 and mito-ribosome gene expression. Cross-referencing eCLIP data, with our
349 polysomal profiling, RNA-seq, RIP results, and GSEA data we compiled a list of fourteen mitoribosomal
350 transcripts as candidate direct DHX30 targets. Interestingly DHX30 and this 14-gene list showed a
351 prognostic significance in cancer types where a positive correlation in their expression was observed.
352 Instead, copy number alterations or mutations in DHX30 were a rare event in cancer (8.6%), were not
353 associated with specific tissue or cancer types, and, although based on a few cases, seemed to be mutually
354 exclusive with mitochondrial genome changes (**Figure S10**).
355 In conclusion, our study demonstrates the role of DHX30 in the coordination between global
356 cytoplasmic translation and mitochondrial functions. This role contributes to the oncogenic potential of
357 cancer cells, and appears to correlate with tumor aggressiveness and clinical outcome. Furthermore, during
358 stress responses activating p53, DHX30 can reduce the apoptotic commitment of cancer cells by acting on
359 specific pro-apoptotic transcripts, thus providing a potential actionable target for therapeutic purposes [6].
360

361 **Materials and Methods**

362 **RNA-seq library preparation and sequencing**

363 shDHX30 and control cells were either kept untreated or treated with 10μM Nutlin, and processed after
364 12h. Polysomal profiling and RNA extraction of reconstituted total cytoplasmic fractions was performed
365 as recently described [6]. Sequencing libraries were obtained following the manufacturer instructions of the
366 TruSeq RNA Library preparation kit v2. We used 1.5 μg of RNA as input, and assessed the input RNA
367 quality by the Agilent RNA 6000 Nano kit on a Agilent 2100 Bioanalyzer instrument. Four replicates were
368 generated for each condition. The resulting 16 samples were sequenced on a HiSeq 2500 machine producing
369 ~25M raw reads per each sample.

370

371 **RNA-seq data analysis**

372 Reads were first quality filtered and trimmed with trimmomatic (minimum quality 30, minimum length
373 36nt) [35]. Then, each Gencode v27 (http://www.gencodegenes.org/releases/) transcript was quantified

374 with Salmon [36]. Eventually, edgeR [37] was used to call Differentially Expressed Genes (DEGs) between
375 conditions at the polysomal and total levels (shDHX30 DMSO vs shNT DMSO), using a 0.05 threshold on
376 the adjusted p-value. GSEA was performed with the fgsea R package [8], including the Hallmark, Canonical
377 Pathways, and GO gene sets. We used 1000 permutations to compute the significance p-value and used a
378 BH adjusted p-value threshold of 0.05. Translational efficiency (TE) was computed on normalized
379 expression data (counts per million reads, CPM) as the ratio of polysomal CPMs over total CPMs for each
380 replicate and transcript in the annotation. Differences in TE (between conditions and groups of genes) and
381 between polysomal and total samples were assessed by the Wilcoxon test. Motifs in ribosomal and
382 mitoribosomal genes 5'- and 3'-UTRs were obtained with DREME [38] using a 1.0E-04 p-value threshold
383 and shuffled input sequences as controls.

384

385 **Cell lines and culture conditions**

386 HCT116 and U2OS shNT control or shDHX30 clones were obtained as recently described [6]. Briefly,
387 cells were transduced with lentiviral vectors containing a pLK0.1 plasmid expressing shRNAs. DHX30
388 targeting sequences are: TRCN0000052028 (GCACACAAATGGACCGAAGAA) TRCN0000052031
389 (CCGATGGCTGACGTATTTCAT), TRCN0000052032 (GAGTTGTTTG ACGCAGCCAAA). Stable
390 clones were selected exploiting the puromycin resistance marker. Single clone isolates were obtained and
391 characterized for DHX30 protein depletion. Consistent results were obtained using the three different
392 shRNAs HCT116 $p53^{-/-}$ cells were obtained from the Vogelstein lab (Sur S. et al, 2009). MCF7 cells were
393 purchased from ICLC (IRCCS San Martino Hospital, Genoa, Italy). All cell lines were cultured in RPMI
394 (Gibco, Thermo Fisher Scientific, Waltham, MA, USA) supplemented with 10% Fetal Bovine Serum
395 (Gibco, Thermo Fisher Scientific), 1X L-Glutamine and Pen/Strep (Gibco, Thermo Fisher Scientific) at 37
396 °C with 5% CO2 in a humidified atmosphere. U2OS cells were cultured in DMEM pH 7.4 (Gibco, Thermo
397 Fisher Scientific) supplemented with 10% Fetal Bovine Serum (Gibco, Thermo Fisher Scientific), 1X L-
398 Glutamine and Pen/Strep (Gibco, Thermo Fisher Scientific) at 37 °C with 5% CO2 in a humidified
399 atmosphere. For routine culture of depleted clones and controls, 0.2 µg/mL Puromycin was added to the
400 culture medium to maintain selection of the vectors. Puromycin was removed 24 hours before starting a
401 specific experiment to avoid confounding effects. MCF-7, U2OS and HCT116 parental and $p53^{-/-}$ cells were

402 silenced for cytoplasmic or cytoplasmic + mitochondrial DHX30 variants using 25nM siRNAs (Trifecta,
403 IDT, Coralville, IA, USA) (**Table S2**) transfected with Interferin (Polyplus-transfection, Illkirch, France).
404 All experiments were performed at least 24 hours post-silencing.
405
406 **Western Blot**
407 Cells were cultured in 6-well tissue culture plates. Cells were collected with trypsin-EDTA after 24 hours,
408 centrifuged and washed with PBS. Samples were then lysed with RIPA buffer and the proteins were
409 quantified by BCA assay (EUROCLONE, Milan, Italy). 30 µg of extracted proteins were loaded on 12%
410 or 15% Tris-glycine Gel and then transferred onto a nitrocellulose membrane using Tris-Glycine buffer.
411 Blocking was performed overnight with 5% not-fat dry milk, 0.1% TWEEN and PBS 1X. Immunodetection
412 was obtained using primary and secondary antibodies reported in **Table S3**. Membranes were analyzed by
413 ECL and detected with ChemiDocTM XRS+ (Bio-Rad, Hercules, CA, USA) using ImageLab software
414 (Bio-Rad).
415
416 **Polysome profiling**
417 Polyribosome analysis was performed as described in [39–41]. Briefly, HCT116 cells were grown on 15
418 cm Petri dishes with standard media and serum. When the cells reached 80% of confluence, cycloheximide
419 (0.01 mg/ml, Sigma Aldrich) was added and kept in incubation for 10 min. Then cells were washed two
420 times with cold PBS containing cycloheximide (0.01 mg/ml) and lysed with the following lysis buffer: 20
421 mM Tris-HCl (pH 7.5), 100 mM KCl, 5 mM MgCl2, 0.5% Nonidet P-40, 100 U/ml RNase inhibitors.
422 Mitochondria and nuclei-free lysates were loaded onto 15–50% (w/v) density sucrose gradients in salt
423 solution (100 mM NaCl, 5 mM MgCl2, 20 mM Tris–HCl pH 7.5), and ultracentrifuged at 180 000 × g for
424 100 min at 4°C. The sedimentation profiles were monitored by absorbance at 254 nm using a Teledyne
425 ISCO UA-6 fractionator coupled to UV detector, collecting thirteen 1 ml fractions. RNA from pooled
426 polysomal fraction was extracted and processed as described in [6]. For Western blot analysis, 100 ul of
427 100% TCA and 1 ml of ice-cold acetone were added to 1 ml of each fraction. Then samples were put at −80
428 °C overnight to induce protein precipitation. Subsequently samples were centrifuged at 16,000 × g for 10

429 min at 4 °C and washed three times with 1 mL of ice-cold acetone. Finally, the pellets were solubilized
430 directly in Laemmli buffer pH 8.
431
432 **Ribosome isolation**
433 Ribosome isolation was performed following a protocol previously described [42]. Briefly, 8 x 10^6 cells
434 were seeded in a T150 flask, 48 hours before the procedure. At 80% of confluence, cells were detached and
435 counted. 1 x 10^7 cells were pelleted by 500 x g centrifugation for 5 minutes at 4°C and washed once with
436 cold PBS. Supernatant was discarded and the pellet was resuspended gently with 300µL of cold buffer A
437 (sucrose 250mM, KCl 250mM, MgCl2 5mM, and Tris-Cl 50 mM pH 7.4), added in three sequential steps,
438 pipetting after every addition. To perform cell lysis, an appropriate volume of NP-40 was added to the
439 homogenized cellular solution, in order to obtain a 0.7% (v/v) final concentration of the detergent, and cells
440 were incubated on ice for 15 minutes, homogenizing the suspension by gentle pipetting every 5 minutes.
441 Then the cell lysate was centrifuged at 750 x g for 10 minutes at 4°C to pellet nuclei; the recovered
442 cytoplasmic fraction (supernatant) was centrifuged again at 12.500 x g for 10 minutes at 4°C to obtain a
443 mitochondria pellet. Supernatant containing ribosomes was collected and its volume was accurately
444 measured using a graduated pipet. KCl 4M solution was then slowly added in order to reach a final
445 concentration of 0.5M. Meanwhile, 1mL of the sucrose cushion solution (sucrose 1M, KCl 0.5M, MgCl2
446 5mM and Tris-Cl 50mM pH 7.4) was added into 3-mL polycarbonate tube for an ultracentrifuge TL100.3
447 rotor (Beckman Coulter, Brea, CA, USA). The KCl-adjusted ribosome-containing solution was carefully
448 added above the sucrose cushion and tubes were balanced by weight using buffer B (sucrose 250mM, KCl
449 0.5M, MgCl2 5mM and Tris-Cl 50mM pH 7.4). Then, they were ultracentrifuged at 250.000 x g for 2 hours
450 at 4°C. At the end of the centrifugation, the supernatant was discarded and a very compact and dense
451 translucent pellet containing ribosomes was quickly rinsed twice by carefully adding 200µL of cold water.
452 Then, pellet was resuspended in 300µL of buffer C (KCl 25mM, MgCl2 5mM and Tris-Cl 50mM pH 7.4),
453 adding the solution in three sequential steps and gently homogenized by pipetting after every 100µL
454 addition. Finally, to estimate the amounts of ribosomes, absorbance at 260nm of the suspensions was
455 measured by a nanodrop spectrophotometer (ThermoFisher).
456

457 **Global Translation**

458 Global translation assay was performed using Click-iT® AHA Alexa Fluor® 488 Protein Synthesis HCS
459 Assay (Thermo Fisher Scientific). Briefly, HCT116 shNT and shDHX30 cells were cultured in 96-well
460 tissue culture plate and treated with 100mM 5-Fluorouracil (Sigma Aldrich) as positive control. After 24
461 hours of treatment, the culture medium was removed and 50µM L-azidohomoalanine prepared in pre-
462 warmed L-methionine-free medium (Lonza) was added and cells were incubated for 1 hour. Cell fixation
463 was performed using 3.7% formaldehyde (Sigma Aldrich) incubating the plate at room temperature for 15
464 minutes. After two washing with 3% BSA in PBS 1X cells were permeabilized with 0.5% Triton® X-100
465 (Sigma Aldrich) and incubated for 15 minutes at room temperature. Cells were washed twice with 3% BSA
466 in PBS 1X and Click-iT® reaction cocktail was added incubating for 30 minutes at room temperature,
467 protected from light. After the incubation reaction cocktail was removed, cells were washed twice with 3%
468 BSA in PBS 1X and stained with 5µg/mL Hoechst (Sigma Aldrich). Samples' images were acquired and
469 analysed by high content fluorescence microscope Operetta® (PerkinElmer, Waltham, MA, USA) using the
470 following filter set: Alexa Fluor® 488: Ex495/Em519 nm; Hoechst: Ex350/Em461 nm.

471

472 **Fluorescent In Situ Hybridization (FISH) on rRNA precursors**

473 Cells were cultured on a coverslip place onto a 48-well plate and after 48 hours they were washed with PBS
474 and fixed with 4% Paraformaldehyde (PFA) (Sigma Aldrich) for 30 minutes at RT. Then, cells were washed
475 twice with PBS 1X and incubated in 70% ethanol overnight at 4°C. The day after, cells were rehydrated
476 with 10% formamide in 2X SSC (Sigma Aldrich), twice for 5 minutes at RT. Meanwhile, buffer A [5µL
477 formamide, 2.5µL SSC 2X, 2.5µL tRNA (10 ng/µL), water up to 20.25µL and then 2.5µL of each probe
478 (10 ng/µL)] was incubated for 5 minutes at 90°C and then mixed quickly together with buffer B [25µL
479 Dextran sulfate 20% in SSC 4X, 1.25µL Bovine Serum Albumin (BSA) (10ng/µL) and 2.5µL
480 ribonucleoside vanadyl complex (RVC) (200mM)]. Then, 50µL A+B probe solution was dropped onto the
481 coverslip and it was incubated in a humidified chamber for 3 hours at 37°C. When the incubation was
482 finished, the coverslip was washed twice with 10% formamide in SSC 2X for 30 minutes at RT and once
483 with PBS 1X for 5 minutes. Cells were stained with a solution of 0.5µg/mL DAPI (Sigma Aldrich) in PBS
484 1X for 5 minutes, washed three times with PBS 1X and the coverslip was finally placed with mounting

485 medium on glass slide. Finally, images were acquired using Zeiss Observer z1 fluorescent microscope (Carl
486 Zeiss, Oberokochen, Germany) with ZEN 2 blue edition software ver. 2.3 (Carl Zeiss). Images'
487 fluorescence intensity was measured using Cell Profiler software ver. 3.1.9 (Broad Institute, Cambridge,
488 MA, USA).
489
490 **rRNA biogenesis**
491 rRNA biogenesis was performed following the protocol described by [43,44]. Briefly, cells were cultured
492 in 96-well tissue culture plates and after 24 hours were treated with Actinomycin D 100nM (Sigma Aldrich)
493 as positive control. After 24 hours of treatment, 1mM 5-Ethynyluridine (Sigma Aldrich) was added to the
494 culture medium and the plate was incubated for 2 hours. This short incubation with 5-EU allows a higher
495 rate of incorporation in rRNAs than mRNAs, reducing the background signal. Then, cells were fixed using
496 a working solution 1 (WR1) composed by 125mM Pipes pH 6.8 (Sigma Aldrich), 10mM EGTA (Sigma
497 Aldrich), 1mM MgCl2 (Merck Millipore, Burlington, MA, USA), 0.2% Triton® X-100 (Sigma Aldrich)
498 and 3.7% formaldehyde (Sigma Aldrich). Cells were washed twice with TBS 1X and stained for 30 minutes
499 at room temperature using a working solution 2 (WR2) composed by 100mM Tris-HCl pH 8.5 (Sigma
500 Aldrich), 1mM CuSO4 (Merck Millipore), 10µM fluorescent azide (Sigma Aldrich) and 100mM ascorbic
501 acid (Merck Millipore). After four washes with TBS containing 0.5% Triton X-100, cells were stained with
502 0.5µg/mL Hoechst (Sigma Aldrich) and samples' images were acquired and analysed by high content
503 fluorescent microscope Operetta® (PerkinElmer) using the following filter set: Alexa Fluor® 488:
504 Ex495/Em519 nm; Hoechst: Ex350/Em461 nm and setting a threshold on Alexa Fluor® 488 at 500
505 fluorescent units to plot the percentage of cells with high nucleolar signal intensity.
506
507 **Colony formation**
508 $1.0x10^3$ HCT116 shNT and shDHX30 cells per well were seeded in a 6-well plate and incubated. Culture
509 medium was changed every three days. Colonies were ex fixed with 3.7% formaldehyde and stained with
510 a solution containing 30% Methylene blue (Sigma Aldrich) in water, then washed five times for 5 minutes.
511 Images were acquired and analysed using ImageJ software 1.8.0 (National Institute of Health, Bethesda,
512 MD, USA).

513

514 **Cell Count in High-Content analysis and Real Time Cell Index Analysis**

515 To analyze cell proliferation by cell count, $1.0x10^3$ cells per well were seeded in 96-well plates and
516 incubated. Images were acquired by high content fluorescent microscope Operetta® (PerkinElmer) in digital
517 phase contrast for three days. To analyse cell proliferation by Real Time Cell Analyser xCELLigence®
518 (RTCA) (Roche, Basel, Switzerland) the background was set adding the only cell culture medium in each
519 well of E-plate and incubating 30 minutes. After incubation, background was read. Then $1.0x10^3$ cells per
520 well were seeded and incubated for 30 minutes and then the E-plate was inserted in the RTCA and
521 impedance-based cell proliferation was estimated by RTCA readings every 15 minutes in the course of
522 three days.

523

524 **Spheroid assay formation**

525 $3.0x10^3$ HCT116 shNT and shDHX30 cells per well were seeded in U-bottom ultra-low attachment 96-well
526 plate (Corning Incorporated, Corning, NY, USA), centrifuged at 3000 rpm for 5 minutes and incubated.
527 Starting after three days of incubation, images were acquired every 24 hours for eight additional days by
528 microscope (Leica, Wetzlar, Germany). Spheroids' area was measured by ImageJ software.

529

530 **Immunofluorescence**

531 $3.0x10^5$ cells per well were seeded on glass coverslip inserted in 6-well plates and incubated overnight. The
532 days after, cells were fixed in 4% Paraformaldehyde (PFA) for 15 min. Then the PFA solution was removed
533 and cells were rinsed twice with PBS 1X. After washing, cells were incubated for 1 hour with blocking
534 solution (PBS 1X, 5% BSA and 0.5% Triton X-100). Next, cells were incubated overnight at 4°C with
535 primary antibodies (Table 2.4) diluted in blocking solution. The following day, after three washes with PBS
536 1X, the anti-mouse and anti-rabbit secondary antibodies conjugated with AlexaFluor 488 or AlexaFluor
537 594 (Invitrogen, Carlsbad, CA, USA) (diluted 1:1000) were added to the samples and incubated for 1 hour
538 at RT under agitation. Cells were washed with PBS 1X three times and cell nuclei were stained with
539 0.5µg/mL Hoechst (Sigma Aldrich) (diluted 1:5000). Finally, coverslips were mounted on glass slides and

540 images were acquired using Zeiss Observer Z1 fluorescent microscope and Zen 2012® software (Carl Zeiss
541 Jena, Germany). The list of primary antibodies used are reported in **Table S3**.
542
543 **Compensatory Glycolytic Test**
544 $3.0x10^3$ cells per well were seeded in Xfp cell culture microplate (Agilent Technologies, Santa Clara, CA,
545 USA) and incubated overnight while XF calibrant solution was added in each well of extracellular flux
546 cartridge and incubated overnight without CO_2. The day after, culture media was removed from cells,
547 replaced with assay medium and microplate was incubated 45 minutes at 37°C without CO_2. Extracellular
548 flux cartridge was prepared adding 0.5µM rotenone/antimycin A in port A and 50mM 2-Deoxyglucose in
549 port B diluted in Xfp assay medium and the cartridge was calibrated by Seahorse XFp analyser setting
550 Glycolysis Test program. When the calibration was finished, cell microplate was inserted in a Seahorse
551 XFp analyser starting the analysis.
552
553 **RNA extraction and qRT-PCR**
554 $3.0x10^5$ cells per well were seeded in a 6-well plate and incubated overnight. The day after, cells were
555 starved and lysed with β-mercaptoethanol and RNA was extracted using Illustra RNAspin Mini RNA
556 Isolation kit (GE-Healthcare, Chicago, IL, USA) following the kit protocol. Then, RNA was retro-
557 transcribed using the RevertAid RT Kit (Thermo Fisher Scientific). Finally, RT-qPCR was performed using
558 25ng and 2x qPCR SyGreen (PCR Biosystem, London, England) in Cfx96™ Real-Time System or
559 Cfx384™ Real-Time System Thermocyclers (Bio-Rad). The sequence of all primers used is reported in
560 **Table S2**.
561
562 **Digital droplet PCR**
563 Digital droplet PCR was performed based on the protocol developed by Bio-Rad. Briefly, $1x10^5$ cells were
564 seeded in 6-well plate and grown for 1 day. Next cells were detached, counted and solubilized in
565 DireCtQuant 100ST solubilization reagent (DireCtQuant, Lleida, Spain) at the concentration of 1000
566 cells/µL, incubating for 3 minutes at 90°C with shaking at 750 rpm and then centrifuged for 1 minute at
567 10000 g. Lysates were obtained by incubation for 3 minutes at 90°C under shaking at 750 rpm and then

568 centrifuged for 1 minute at 10000 g. Lysate was diluted 1:4 in solubilization reagent and for every target to
569 analyze, PCR mix was prepared comprising 2µL of diluted sample, forward and reverse primers at 10µM
570 final concentration in a final volume of 95µL. PCR mix without lysate was used as negative control. Then,
571 10.5µL of each PCR reaction was mixed with 11µL of 2xQX200 ddPCR EvaGreen SuperMix (Bio-Rad)
572 and 0.5µL of HindIII restriction enzyme (NEB, Ipswich, MA, USA). Sample DNA was digested at 37°C
573 for 15 minutes and loaded in ddPCR DG8™ Cartridge with QX200™ droplet generation oil (Bio-Rad).
574 Droplets were made using QX200™ droplet generator (Bio-Rad) and then loaded in a 96-well PCR plate.
575 Sample DNA was amplified and finally, droplets with amplified DNA were analyzed using the QX200™
576 droplet reader and QuantaSoft 1.7.4 (Bio-Rad).
577
578 **RNA Immunoprecipitation**
579 HCT116 cells were cultured in standard medium in P150 plates till they reached ~80% confluence. ~10^7
580 cells were lysed in 1mL of Lysis buffer (100mM KCl, 5mM $MgCl_2$, 10mM HEPES pH 7, 0.5% NP-40,
581 1mM DTT, 1U/ul RNase Inhibitors, 1X Protease Inhibitor Cocktail) using a scraper. Lysates were
582 transferred in a falcon tube, placed for at least two hours at -80°C, and centrifuged at 10000 rpm for 30
583 minutes. Supernatants were collected in a new tube. Dynabeads ProteinA or ProteinG (depending on the
584 antibody species, Thermo Fisher scientific) were prepared by washing them twice with NT2 Buffer (50mM
585 Tris-HCl pH7.4, 150mM NaCl, 1mM $MgCl_2$; 0.05% NP40) and resuspended in NT2 buffer. Beads were
586 distributed in different tubes, supplemented with twice their initial volume of NT2 Buffer. The DHX30
587 specific antibody (5 µg -A302-218A, Bethyl) or IgGs were added to the beads and incubated for 2 hours
588 on a rotating wheel at 4°C. Lysates were pre-cleared by adding a mix containing ProteinA and ProteinG
589 Dynabeads in equal amounts and incubating for 1 hour at 4°C on a wheel. After placing the tubes on a
590 magnet, supernatants were collected and 1% of their volume was used as input to be directly extracted with
591 TRIzol. The remaining supernatant was added to the antibody-coated beads and incubated overnight on a
592 wheel at 4°C. The day after, beads were washed with 1ml NT2 buffer for 10 minutes on a wheel at 4°C.
593 Three additional washes were performed again with 1ml NT2 Buffer supplemented with 0.1% Urea +
594 50mM NaCl (10 minutes each at 4°C on a wheel). Beads were washed one more time in 500µl of NT2
595 buffer, 50µl were collected for WB analysis and the remaining supernatant was discarded. RNA was

596 extracted by adding TRIzol to the beads, according to the manufacturer's protocol. The RNA pellets were
597 resuspended in 15µl DEPC water and cDNAs were synthesized using the RevertAid First Strand cDNA
598 Synthesis Kit (Thermo Fisher Scientific).
599
600 **Cytoplasm-Mitochondria fractionation**
601 For cytoplasm-mitochondria fractionation, $2x10^6$ cells were seeded in a P150 Petri dish and incubated for
602 2 day. Then, they were detached using trypsin and re-suspended in 750µL of Mitochondrial Isolation Buffer
603 (MIB) (0.32M Sucrose, 1mM EGTA pH 8.0, 20mM Tris-HCl pH 7.2) with 0.1% fatty acid-free BSA. Cells
604 were homogenized in a Potter-Elvehjem homogenizer (DWK Life Sciences, Mainz, Germany) applying
605 more than 60 strokes. Homogenate (A) was centrifuged for 5 minutes at 1000g at 4°C and supernatant was
606 collected. Cell debris were resuspended in 750µL of MIB + BSA and re-homogenized with more than 20
607 strokes. New homogenate (B) was centrifuged for 5 minutes at 1000g at 4°C and the supernatant was
608 collected and pooled with supernatant A. Two mixed supernatants (A+B) were centrifuged at 12000g for
609 10 minutes at 4°C to pellet the mitochondria. Supernatant was discarded and mitochondria were washed
610 twice with 1mL of MIB + BSA and once with 1mL of MIB, centrifuging the mitochondrial pellet every
611 time at 12000g for 10 minutes at 4°C. Finally, supernatant was discarded and mitochondria were lysed in
612 RIPA buffer and mitochondrial proteins were quantified by BCA assay.
613
614 **Apoptosis assay**
615 Apoptosis analysis was based on FITC Annexin-V Apoptosis Detection Kit protocol (BD Biosciences, San
616 Jose, CA, USA). Briefly, $3x10^5$ cells per well were seeded in a 6-well plate, incubated for one day and then
617 treated with drugs under investigation for 48 hours. 0.1% DMSO was used as negative control. Cells were
618 detached using trypsin and washed twice with PBS 1X. Then, $1.5x10^5$ cells were resuspended in 100µL of
619 Binding Buffer 1X, stained with FITC-Annexin V and PI and incubated for 15 minutes at room temperature
620 in the dark. Finally, samples were analyzed by FACSCanto™ flow cytometer and BD Diva Software 6.1.3.
621 Unstained, PI-only and FITC-only stained samples were used to set the cytometer's parameters.
622
623 **Cell cycle analysis**

624 HCT shNT or shDHX30 were seeded in 6-well plates at a concentration of $3x10^5$ cell/well. 48 hours after
625 seeding, cells were trypsinized, washed with 1X PBS and counted for subsequent staining according to BD
626 Cycletest™ Plus DNA Kit protocol. Briefly, $5x10^5$cells were centrifuged, superantant was removed and
627 250µl of Solution A were added. Cells were resuspended and incubated for 10 minutes before adding 200
628 µl of Solution B. After 10 minutes of incubation, 200 µl of ice-cold Solution C were added to the samples
629 and cells were incubated for 10 minutes at 4°C in the dark before analysis with FACS CantoA (BD). The
630 percentage of cells in each stage of the cell cycle (G1, S or G2) was computed using the ModFIT LT 4.0
631 software (Verity Software House).
632

633 **Exploration of TGCA data using the GEPIA web resource**

634 The GEPIA API [17,18] was used to extract correlations between DHX30 and mitoribosomal genes (either
635 as individual genes or for the 14-genes signature) in all available TCGA tumor datasets (correlation mode).
636 The same analysis was performed to correlate cytoplasmic ribosome and mitochondrial ribosome genes
637 expression, on TCGA tumor samples, matched TCGA normal samples, and GTEX healthy tissues RNA-
638 seq data. Survival analysis was performed with the same tool and in the same datasets, using the survival
639 mode. Only results within the p-value threshold of 0.05 were considered, with the others being set to R=0
640 and HR=1 in the heatmap for visualization purposes.

641 **Statistical analysis**

642 Data are presented as mean ± SD of three independent biological experiments, unless stated otherwise.
643 GraphPad Prism 5 or 9 software (GraphPad software, La Jolla, CA, USA) were used and either a two-way
644 anova with Tukey's multiple comparison test or a two-tailed Student's t-test was performed, unless
645 specified otherwise.
646

647 **Data availability**

648 The RNA-seq datasets are available in GEO with ID GSE95024 and GSE154065.
649

Acknowledgements

We thank Pamela Gatto, Viktoryia Sirarovich and Michael Pancher of the HTS CIBIO core facility for assistance with droplet digital PCR experiments, high-content as well as impedance-based proliferation assays. We thank Nicoletta di Bernardo for technical assistance for the apoptosis assays. This work was supported by the Italian Association for Cancer Research (Fondazione AIRC, IG grant #18985 to AI). JJD laboratory is supported by grants by the Institut National du Cancer (INCa, grant PRT-K program n°2018-024 EMT-CoNCEPT) and Agence Nationale de la Recherche (ANR, grant RiboCard ANR-18-CE11-0020, and grant ActiMeth ANR-19-CE12-0004).

Competing Interests

The Authors declare no competing interest.

Authors contributions

B.B. perfomed most experiments and wrote the first draft of the paper. A.R., D.R., S.G., A.P., F.B., and, A.G. helped in some experimental procedures. F.C. and J-J.D. helped to design some experiments. E.D. performed all data analysis. E.D. and A.I. designed the study. A.I. co-wrote the first draft of the manuscript.

References

1. Zheng HJ, Tsukahara M, Liu E, Ye L, Xiong H, Noguchi S, et al. The novel helicase helG (DHX30) is expressed during gastrulation in mice and has a structure similar to a human DExH box helicase. Stem Cells Dev. 2015;24: 372–383. doi:10.1089/scd.2014.0077
2. Ye P, Liu S, Zhu Y, Chen G, Gao G. DEXH-Box protein DHX30 is required for optimal function of the zinc-finger antiviral protein. Protein Cell. 2010; doi:10.1007/s13238-010-0117-8
3. Lessel D, Schob C, Kury S, Reijnders MRF, Harel T, Eldomery MK, et al. De Novo Missense Mutations in DHX30 Impair Global Translation and Cause a Neurodevelopmental Disorder. Am J Hum Genet. 2017;101: 716–724. doi:10.1016/j.ajhg.2017.09.014
4. Antonicka H, Shoubridge EA. Mitochondrial RNA Granules Are Centers for Posttranscriptional RNA Processing and Ribosome Biogenesis. Cell Rep. 2015;10: 920–932. doi:10.1016/j.celrep.2015.01.030
5. Andrysik Z, Galbraith MD, Guarnieri AL, Zaccara S, Sullivan KD, Pandey A, et al. Identification of a core TP53 transcriptional program with highly distributed tumor suppressive activity. Genome Res. 2017;27. doi:10.1101/gr.220533.117
6. Rizzotto D, Zaccara S, Rossi A, Galbraith MD., Andrysik Z, Pandey A, et al. Nutlin-Induced Apoptosis is Specified by a Translation Program Regulated by PCBP2 and DHX30. Cell Rep. 2020;30: 1–15.
7. Tovar C, Rosinski J, Filipovic Z, Higgins B, Kolinsky K, Hilton H, et al. Small-molecule MDM2 antagonists reveal aberrant p53 signaling in cancer: implications for therapy. Proc Natl Acad Sci U S A. 2006;103: 1888–1893. doi:10.1073/pnas.0507493103
8. Sergushichev AA. An algorithm for fast preranked gene set enrichment analysis using cumulative

690 statistic calculation. bioRxiv. 2016; doi:10.1101/060012
691 9. Van Nostrand EL, Pratt GA, Shishkin AA, Gelboin-Burkhart C, Fang MY, Sundararaman B, et al.
692 Robust transcriptome-wide discovery of RNA-binding protein binding sites with enhanced CLIP
693 (eCLIP). Nat Methods. 2016;13: 508–514. doi:10.1038/nmeth.3810
694 10. Mills EW, Green R. Ribosomopathies: There's strength in numbers. Science. 2017. p. eaan2755.
695 doi:10.1126/science.aan2755
696 11. Wang Y, Bogenhagen DF. Human mitochondrial DNA nucleoids are linked to protein folding
697 machinery and metabolic enzymes at the mitochondrial inner membrane. J Biol Chem. 2006;281:
698 25791–802. doi:10.1074/jbc.M604501200
699 12. Smith AC, Robinson AJ. MitoMiner v3.1, an update on the mitochondrial proteomics database.
700 Nucleic Acids Res. Oxford University Press; 2016;44: D1258–D1261. doi:10.1093/nar/gkv1001
701 13. Armenteros JJA, Salvatore M, Emanuelsson O, Winther O, Von Heijne G, Elofsson A, et al.
702 Detecting sequence signals in targeting peptides using deep learning. Life Sci Alliance. Rockefeller
703 University Press; 2019;2. doi:10.26508/lsa.201900429
704 14. Fazal FM, Han S, Parker KR, Kaewsapsak P, Xu J, Boettiger AN, et al. Atlas of Subcellular RNA
705 Localization Revealed by APEX-Seq. Cell. 2019; doi:10.1016/j.cell.2019.05.027
706 15. Heiden MGV, Cantley LC, Thompson CB. Understanding the warburg effect: The metabolic
707 requirements of cell proliferation. Science. 5930: 1029-1033; 2009. p. 324.
708 doi:10.1126/science.1160809
709 16. Schwanhüusser B, Busse D, Li N, Dittmar G, Schuchhardt J, Wolf J, et al. Global quantification of
710 mammalian gene expression control. Nature. 2011;473: 337–342. doi:10.1038/nature10098
711 17. Tang Z, Li C, Kang B, Gao G, Li C, Zhang Z. GEPIA: A web server for cancer and normal gene
712 expression profiling and interactive analyses. Nucleic Acids Res. 2017;45: W98–W102.
713 doi:10.1093/nar/gkx247
714 18. Tang Z, Kang B, Li C, Chen T, Zhang Z. GEPIA2: an enhanced web server for large-scale
715 expression profiling and interactive analysis. Nucleic Acids Res. 2019;47: W556–W560.
716 doi:10.1093/nar/gkz430
717 19. Wieser W, Krumschnabel G. Hierarchies of ATP-consuming processes: Direct compared with
718 indirect measurements, and comparative aspects. Biochem J. 2001; 389–95. doi:10.1042/0264-
719 6021:3550389
720 20. Buttgereit F, Brand MD. A hierarchy of ATP-consuming processes in mammalian cells. Biochem
721 J. 1995; 163–7. doi:10.1042/bj3120163
722 21. Couvillion MT, Soto IC, Shipkovenska G, Churchman LS. Synchronized mitochondrial and
723 cytosolic translation programs. Nature. 2016;533: 499–503. doi:10.1038/nature18015
724 22. Calamita P, Gatti G, Miluzio A, Scagliola A, Biffo S. Translating the game: Ribosomes as active
725 players. Front Genet. 2018;15: 533. doi:10.3389/fgene.2018.00533
726 23. Pla-Martín D, Schatton D, Wiederstein JL, Marx M, Khiati S, Krüger M, et al. CLUH granules
727 coordinate translation of mitochondrial proteins with mTORC1 signaling and mitophagy. EMBO J.
728 2020;39: e102731. doi:10.15252/embj.2019102731
729 24. Morita M, Prudent J, Basu K, Goyon V, Katsumura S, Hulea L, et al. mTOR Controls Mitochondrial
730 Dynamics and Cell Survival via MTFP1. Mol Cell. 2017;67: 922–935.
731 doi:10.1016/j.molcel.2017.08.013
732 25. Clarke K, Ricciardi S, Pearson T, Bharudin I, Davidsen PK, Bonomo M, et al. The Role of Eif6 in
733 Skeletal Muscle Homeostasis Revealed by Endurance Training Co-expression Networks. Cell Rep.
734 2017; doi:10.1016/j.celrep.2017.10.040
735 26. Biffo S, Manfrini N, Ricciardi S. Crosstalks between translation and metabolism in cancer. Current
736 Opinion in Genetics and Development. 2018. doi:10.1016/j.gde.2017.10.011
737 27. Ricciardi S, Manfrini N, Alfieri R, Calamita P, Crosti MC, Gallo S, et al. The Translational
738 Machinery of Human CD4 + T Cells Is Poised for Activation and Controls the Switch from
739 Quiescence to Metabolic Remodeling. Cell Metab. Cell Press; 2018;28: 895-906.e5.
740 doi:10.1016/j.cmet.2018.08.009
741 28. Pourdehnad M, Truitt ML, Siddiqi IN, Ducker GS, Shokat KM, Ruggero D. Myc and mTOR
742 converge on a common node in protein synthesis control that confers synthetic lethality in Myc-
743 driven cancers. Proc Natl Acad Sci U S A. 2013;110: 11988–93. doi:10.1073/pnas.1310230110
744 29. Hong S, Freeberg MA, Han T, Kamath A, Yao Y, Fukuda T, et al. LARP1 functions as a molecular
745 switch for mTORC1-mediated translation of an essential class of mRNAs. Elife. 2017;6: e25237.

746 doi:10.7554/eLife.25237
747 30. Amaldi F, Pierandrei-Amaldi P. TOP genes: a translationally controlled class of genes including
748 those coding for ribosomal proteins. Progress in molecular and subcellular biology. 1997. pp. 1–17.
749 doi:10.1007/978-3-642-60471-3_1
750 31. Gressner O, Schilling T, Lorenz K, Schulze Schleithoff E, Koch A, Schulze-Bergkamen H, et al.
751 TAp63alpha induces apoptosis by activating signaling via death receptors and mitochondria. Embo
752 J. 2005;24: 2458–2471. doi:10.1038/sj.emboj.7600708
753 32. Kissil JL, Deiss LP, Bayewitch M, Raveh T, Khaspekov G, Kimchi A. Isolation of DAP3, a novel
754 mediator of interferon-γ-induced cell death. J Biol Chem. 1995;46: 27932–6.
755 doi:10.1074/jbc.270.46.27932
756 33. Yoo YA, Kim MJ, Park JK, Chung YM, Lee JH, Chi S-G, et al. Mitochondrial Ribosomal Protein
757 L41 Suppresses Cell Growth in Association with p53 and p27Kip1. Mol Cell Biol. 2005;15: 6603–
758 13. doi:10.1128/mcb.25.15.6603-6616.2005
759 34. Kim HJ, Maiti P, Barrientos A. Mitochondrial ribosomes in cancer. Seminars in Cancer Biology.
760 2017. pp. 67–81. doi:10.1016/j.semcancer.2017.04.004
761 35. Bolger AM, Lohse M, Usadel B. Trimmomatic: a flexible trimmer for Illumina sequence data.
762 Bioinformatics. 2014;30: 2114–2120. doi:10.1093/bioinformatics/btu170
763 36. Patro R, Duggal G, Love MI, Irizarry RA, Kingsfor C. Salmonprovides accurate, fast, and bias-
764 aware transcript expression estimates using dual-phase inference. bioRxiv Prepr. 2016;
765 37. Robinson MD, McCarthy DJ, Smyth GK. edgeR: a Bioconductor package for differential expression
766 analysis of digital gene expression data. Bioinformatics. 2010;26: 139–140.
767 doi:10.1093/bioinformatics/btp616
768 38. Bailey TL. DREME: Motif discovery in transcription factor ChIP-seq data. Bioinformatics.
769 2011;15: 1653–1659. doi:10.1093/bioinformatics/btr261
770 39. Provenzani A, Fronza R, Loreni F, Pascale A, Amadio M, Quattrone A. Global alterations in mRNA
771 polysomal recruitment in a cell model of colorectal cancer progression to metastasis.
772 Carcinogenesis. 2006;27: 1323–1333.
773 40. Viero G, Lunelli L, Passerini A, Bianchini P, Gilbert RJ, Bernabò P, et al. Three distinct ribosome
774 assemblies modulated by translation are the building blocks of polysomes. J Cell Biol. 2015;208:
775 581–96. doi:10.1083/jcb.201406040
776 41. Panda A, Martindale J, Gorospe M. Polysome Fractionation to Analyze mRNA Distribution
777 Profiles. BIO-PROTOCOL. 2017;7: e2126. doi:10.21769/bioprotoc.2126
778 42. Belin S, Hacot S, Daudignon L, Therizols G, Pourpe S, Mertani HC, et al. Purification of ribosomes
779 from human cell lines. Current Protocols in Cell Biology. 2010. p. unit 3.40.
780 doi:10.1002/0471143030.cb0340s49
781 43. Cornella N, Tebaldi T, Gasperini L, Singh J, Padgett RA, Rossi A, et al. The hnRNP RALY regulates
782 transcription and cell proliferation by modulating the expression of specific factors including the
783 proliferation marker E2F1. J Biol Chem. 2017;292: 19674–19692. doi:10.1074/jbc.M117.795591
784 44. Rossi A, Moro A, Tebaldi T, Cornella N, Gasperini L, Lunelli L, et al. Identification and dynamic
785 changes of RNAs isolated from RALY-containing ribonucleoprotein complexes. Nucleic Acids Res.
786 2017;45: 6775–6792. doi:10.1093/nar/gkx235
787
788
789
790

Table S1: RNA-seq Fold Change data and results of GSEA analysis for the comparison between HCT_shDHX30 and HCT_shNT.
A), B) ID, gene symbol, fold change, F value, P value and FDR based on RNA-seq data of (A) polysomal RNA, (B) total RNA. GSEA data for polysomal (C) or total (D) RNA-seq data.

Table S2: siRNAs, FISH probe, and primers.
Contains information on all primers used in qRT-PCR experiments.

Table S3: List of primary and secondary antibodies

Figure legends

Figure 1. DHX30 reduces ribosome biogenesis and translation in HCT116 colorectal cancer cells.

A) Most significant terms by Gene Set Enrichment Analysis of the polysome-bound DEGs (HCT_shDHX30 vs HCT sh_NT). Bars plot the Normalized Enrichment Score, (NES). Numbers indicate the number of genes in the leading edge. See Table S1 for full results. **B**) Box plot of Translation efficiency for the indicated transcript groups. The RNA-seq CPM in polysomal over total RNA was measured. Results obtained in HCT116_shDHX30 cells are compared to the shNT control clone ; *$p < 0.05$, ***$p < 0.001$. **C**) Amounts of ribosomes produced in HCT116_shDHX30 and HCT_shNT. After ribosomes isolation, protein absorbance was measured at λ 260nm. Data are normalized on shNT and are mean ± SD (n=3); *$p < 0.05$. **D**) Amount of ribosomal RNA estimated based on the fluorescence intensity of 5-ethynyl uridine (5-EU) incorporated in nascent rRNAs present in the nucleoli. HCT116_shDHX30 cells are compared to the shNT control clone in untreated condition while Actinomycin-D treatment was used as a control. Data are mean ± SD (n=6); ***$p < 0.001$. **E**) (Left) Representative images of one of three independent experiments of Fluorescent In Situ Hybridization (FISH) for rRNA precursor 18S (red). Immunofluorescence of tubulin (green) and staining with DAPI (blue) were used to visualize cells. (Right) Box plot of 18S rRNA intensity quantification comparing HCT116_shDHX30 with HCT_shNT analyzed with Cell Profiler software. Data are expressed as mean per well ± SD of three biological replicates in which 10 nuclei were quantified for each replicate; *$p < 0.05$. **F**) Analysis of global translation based on the fluorescence intensity of L-azidohomoalanine (AHA) incorporated in nascent proteins present in the cytoplasm. HCT116_shDHX30 cells are compared to the shNT control clone in untreated condition while 5-Fluorouracil treatment was used as positive control. Data are mean ± SD (n=6 to 9); ***$p < 0.005$. **G**) (Left) Polysome profiling of

824 HCT_shNT and HCT_shDHX30, revealed by the measurement of absorbance at a wavelength of 260 nm.
825 (Right) Box plot of the relative quantification of the area under the curve of fractions corresponding to the
826 polysomes related to the fractions corresponding to the ribosomal subunits and 80S monosome (POL/SUB,
827 an estimate of translation efficiency). Data are mean ± SD (n=7); *p < 0.05.
828
829 **Figure 2. Cytoplasmic DHX30 modulates the expression of nuclear encoded mito-ribosome**
830 **components MRPL11 and MPRS22.**
831 **A**) RNA immunoprecipitation experiments to study the binding of DHX30 to MRPL11 and MRPS22
832 transcripts. Results obtained with a primary antibody targeting DHX30 (blue) or the control IgG control
833 (grey) are plotted relative as % of input. Data are mean and individual points (n=2); p-value was calculated
834 comparing the amount of each sample with the amount of *RNR1* mRNA; *p < 0.05, ***p < 0.001. **B**)
835 Relative mRNA levels of MRPL11 and MRPS22 in HCT116_shDHX30 compared to the shNT control
836 clone. Data are mean ± SD (n=3); *p < 0.05; **p < 0.01. **C**) (Left) Protein levels of MRPL11 and MRPS22.
837 β-Tubulin was used as loading control. Immunoblots represent one of three independent experiments.
838 (Right) MRPL11 and MRPS22 protein quantification in HCT116_shDHX30 normalized on shNT control
839 clone. Data are mean ± SD (n=3); *p < 0.05. **D**) Representative images of one of three independent
840 immunofluorescence experiments to colocalize DHX30 (red) with MT-ATP6 (green, used as mitochondrial
841 marker). Staining with Hoechst (blue) was used to visualize cells' nuclei. **E**) Relative mRNA levels of
842 cytoplasmic DHX30 (cDHX30) and the mitochondrial variant (mDHX30, set to 1). Data are mean ± SD
843 (n=3); ***p < 0.001. **F**) Relative DHX30 protein levels in cytoplasm and mitochondria. β-Tubulin and MT-
844 ATP6 are used as controls of cytoplasmic-mitochondrial fractionation and Ponceau-S staining is used as
845 loading control. One of three independent experiments is shown.
846
847 **Figure 3. Transient DHX30 silencing leads to enhanced translation but reduced mitorobosome gene**
848 **expression in HCT116 cells.**
849 **A)** qRT-PCR to verify the silencing of DHX30 transcripts in HCT116 96 hours after transient transfection
850 with the indicated siRNAs. The relative mRNA levels of cytoplasmic (cDHX30) and mitochondrial
851 (mDHX30) DHX30 transcripts as well as of total DHX30 (measured with a pair or primers common to all

852 annotated transcripts). Data are mean ± SD (n=3); **p < 0.01; ***p < 0.001. **B)** Global translation based
853 on the fluorescence intensity of L-azidohomoalanine (AHA) incorporated in nascent proteins present in the
854 cytoplasm. HCT116 were transiently transfected with the indicated siRNAs and tested after 96 hours. 5-
855 Fluorouracil treatment was used as control treatment leading to translation inhibition. Data are mean ± SD
856 (n=3); * p < 0.05; **p < 0.01. **C**) mRNA levels of MRPL11 and MRPS22 in HCT116 silenced transiently
857 for cytoplasmic DHX30 (HCT_siDHX30-C) or for both cytoplasmic and mitochondrial variants
858 (HCT_siDHX30-C+M). Data are compared to the siRNA negative control (HCT_siNC) and are mean ±
859 SD (n=3); *p < 0.05. **D**) (Left) MRPL11 and MRPS22 protein levels in HCT116 silenced for cytoplasmic
860 DHX30 (HCT_siDHX30-C) or for both cytoplasmic and mitochondrial variants (HCT_siDHX30-C+M).
861 Immunoblot represents one of three independent experiments. (Right) MRPL11 and MRPS22 protein
862 quantification in HCT116_siDHX30-C and HCT116_siDHX30-C+M normalized on α-actinin and
863 compared to siNC control. Data are mean ± SD (n=3); *p < 0.05.
864
865
866 **Figure 4. Depletion of DHX30 reduces the expression and function of mitochondrially encoded**
867 **OXPHOS components.**
868 **A**) Relative mitochondrial genome copy number in HCT116_shDHX30 and -shNT measured by droplet
869 digital PCR. MT-RNR1 and MT-ATP8 were amplified along with the nuclear diploid marker gene
870 CTDSP1. Bars plot mean ± SD (n=3). **B**) Relative mRNA levels of mitochondrially encoded OXPHOS
871 components in HCT116_shDHX30 compared to HCT116_shNT (dashed line, set to 1). For both upper and
872 lower panel, data are mean ± SD (n=3); *p < 0.05; **p < 0.01. **C**) Protein levels of MT-ATP6 and MT-
873 ATP8 in mitochondrial lysates of HCT116_shDHX30 and the shNT control clone. Ponceau-S was used as
874 loading control. Immunoblots represent one of two independent qualitative comparisons. **D**) Relative
875 mRNA levels of the indicated mitochondrially encoded OXPHOS components in HCT116 transiently
876 silenced for DHX30 expression (siDHX30-C, siDHX30-C+M) compared to siNC (dashed line, set to 1).
877 Data are mean ± SD (n=3); *p < 0.05; **p < 0.01; ***p < 0.001. **E**) (Left) Protein levels of MT-ATP6 and
878 MT-ATP8 in HCT116 transiently silenced as in D). α-actinin was used as loading control. Immunoblots
879 represent one of three independent experiments. (Right) MT-ATP6 and MT-ATP8 protein quantification in

880 HCT116_siDHX30-C and HCT116_siDHX30-C+M normalized on α-actinin and compared to siNC
881 control. Data are mean ± SD (n=3); **p < 0.01; ***p < 0.001. **F**) (Left) Measurement of the oxygen
882 consumption rate (OCR) to evaluate mitochondrial respiration by Seahorse XF analyzer. Points before the
883 Rotenone/Antimycin-A (Rot/AA) treatment correspond to the basal mitochondrial respiration. (Right)
884 Extracellular acidification rate (ECAR) measurement was used as a means to measure glycolysis. Points
885 before and after the Rotenone/Antimycin-A (Rot/AA) treatment correspond respectively to basal and
886 compensatory glycolysis -in response to the block of mitochondrial respiration-. 2-Deoxyglucose (2-DG)
887 is then used to block glycolysis. For both panels, one of three independent replicates is presented. Data are
888 mean ± SD (n=3 wells in the Seahorse cartridge); *p < 0.05.
889
890 **Figure 5. Depletion of DHX30 reduces proliferation and survival in basal and treatment conditions**
891 **A)** (Left) Representative image of colony formation assays. (Right) Colony quantification by ImageJ
892 software. Data are mean ± SD (n=3). **B)** Relative cell proliferation measured by high-content microscopy
893 in digital phase contrast. Data are mean ± SD (n=3). **C)** Estimate of relative proliferation by an impedance-
894 based Real-Time Cell Analyzer. Data are mean ± SD (n=3). **D)** Spheroid formation and growth assay. (Left)
895 A representative image at the indicated time points is shown in the left panel. (Right) Spheroid area
896 measured by ImageJ software. Data are mean ± SD (n=3). **E)** (Left) Representative image of
897 HCT116_shNT and shDHX30 cell cycle profiles. (Right) Quantification of cell cycle profile in HCT116
898 DHX30 depleted cells compared to shNT control. Data are mean ± SD (n=3). **F**) Lef panel: relative
899 expression of eIF2alpha and phosho-eIF2alpha in HCT116 cells stably depleted for DHX30 expression or
900 control. A representative immunodetection image is shown. Right panel: relative average protein
901 quantification and SD of three replicates is presented in the bar graph; n = 3, *p < 0.05. **G)** Relative
902 proliferation measured as in B) but starting 24 hours after transient silencing DHX30 with the indicated
903 siRNAs. **H**) Relative expression of the annexin-V apoptosis markers in cells treated for 48 hours with the
904 indicated drugs or DMSO control. For all panels, data are mean ± SD (n=3); *p < 0.05; **p < 0.01.
905
906 **Figure 6. DHX30 expression positively correlates with the expression of mitoribosomal protein**
907 **transcripts and can have prognostic significance.**

908 The table presents the expression correlation data (R value and p value) between DHX30 and the combined
909 group of 14 mitoribosomal protein transcripts is listed for each cancer type (see also Figure S6). Data from
910 Kaplan-Meier survival analysis for the aggregated 15-gene signature (DHX30 + the 14 mitoribosomal
911 protein transcripts) are shown. Significant differences are highlighted in bold font. The tumor type acronym
912 and extended name are also shown. The graphs below the table presents two examples among the cluster
913 of eleven cancer types where a positive correlation is apparent. Left panels: Pearson correlation. Right
914 panels: Overall Survival Kaplan-Meier. The correlation value, the Hazardous Ratio, p values and sample
915 sizes are shown.
916

Figure 1

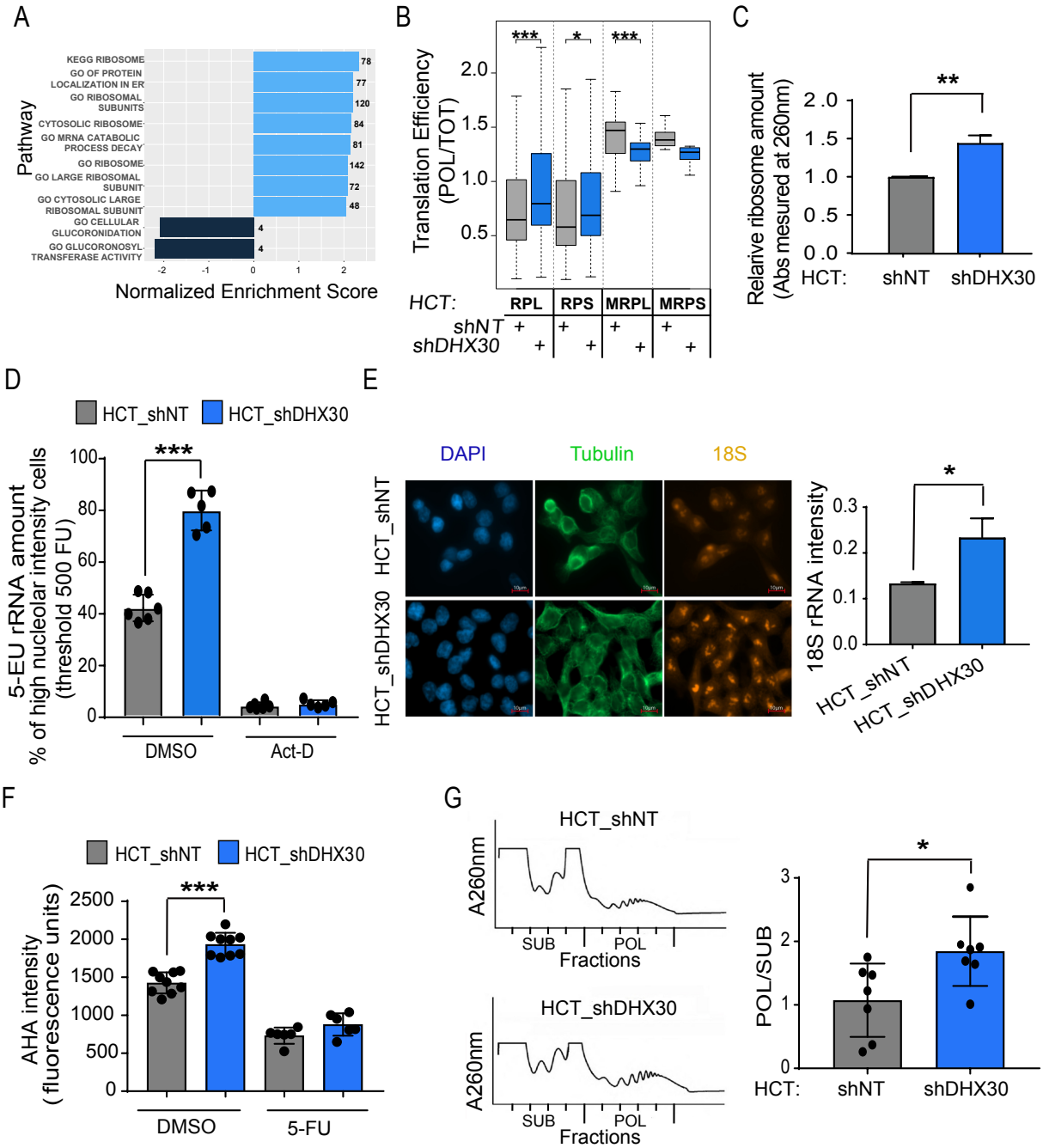
A
Pathway
KEGG RIBOSOME
GO OF PROTEIN LOCALIZATION IN ER
GO RIBOSOMAL SUBUNITS
CYTOSOLIC RIBOSOME
GO MRNA CATABOLIC PROCESS DECAY
GO RIBOSOME
GO LARGE RIBOSOMAL SUBUNIT
GO CYTOSOLIC LARGE RIBOSOMAL SUBUNIT
GO CELLULAR GLUCORONIDATION
GO GLUCORONOSYL TRANSFERASE ACTIVITY
78
77
120
84
81
142
72
48
4
4
-2
-1
0
1
2
Normalized Enrichment Score
B
Translation Efficiency (POL/TOT)
2.0
1.5
1.0
0.5
***
*
***
HCT:
RPL
RPS
MRPL
MRPS
shNT
shDHX30
C
Relative ribosome amount (Abs mesured at 260nm)
2.0
1.5
1.0
0.5
0.0
**
HCT:
shNT
shDHX30
D
HCT_shNT
HCT_shDHX30
5-EU rRNA amount % of high nucleolar intensity cells (threshold 500 FU)
100
80
60
40
20
0
***
DMSO
Act-D
E
DAPI
Tubulin
18S
HCT_shNT
HCT_shDHX30
18S rRNA intensity
0.3
0.2
0.1
0.0
*
HCT_shNT
HCT_shDHX30
F
HCT_shNT
HCT_shDHX30
AHA intensity (fluorescence units)
2500
2000
1500
1000
500
0
***
DMSO
5-FU
G
HCT_shNT
A260nm
SUB
POL
Fractions
HCT_shDHX30
A260nm
SUB
POL
Fractions
POL/SUB
3
2
1
0
*
HCT:
shNT
shDHX30

919 Figure 2

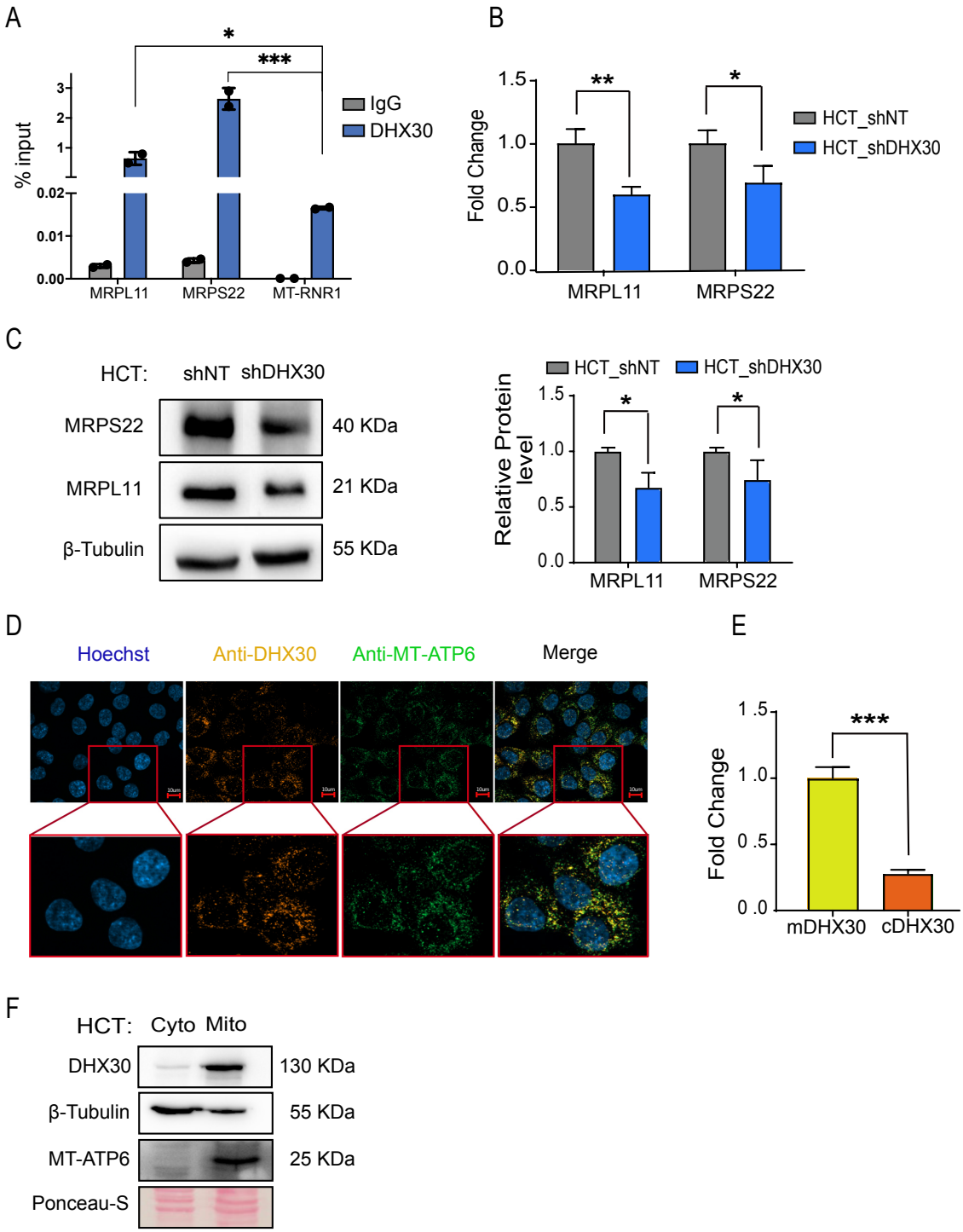

920

921 Figure 3

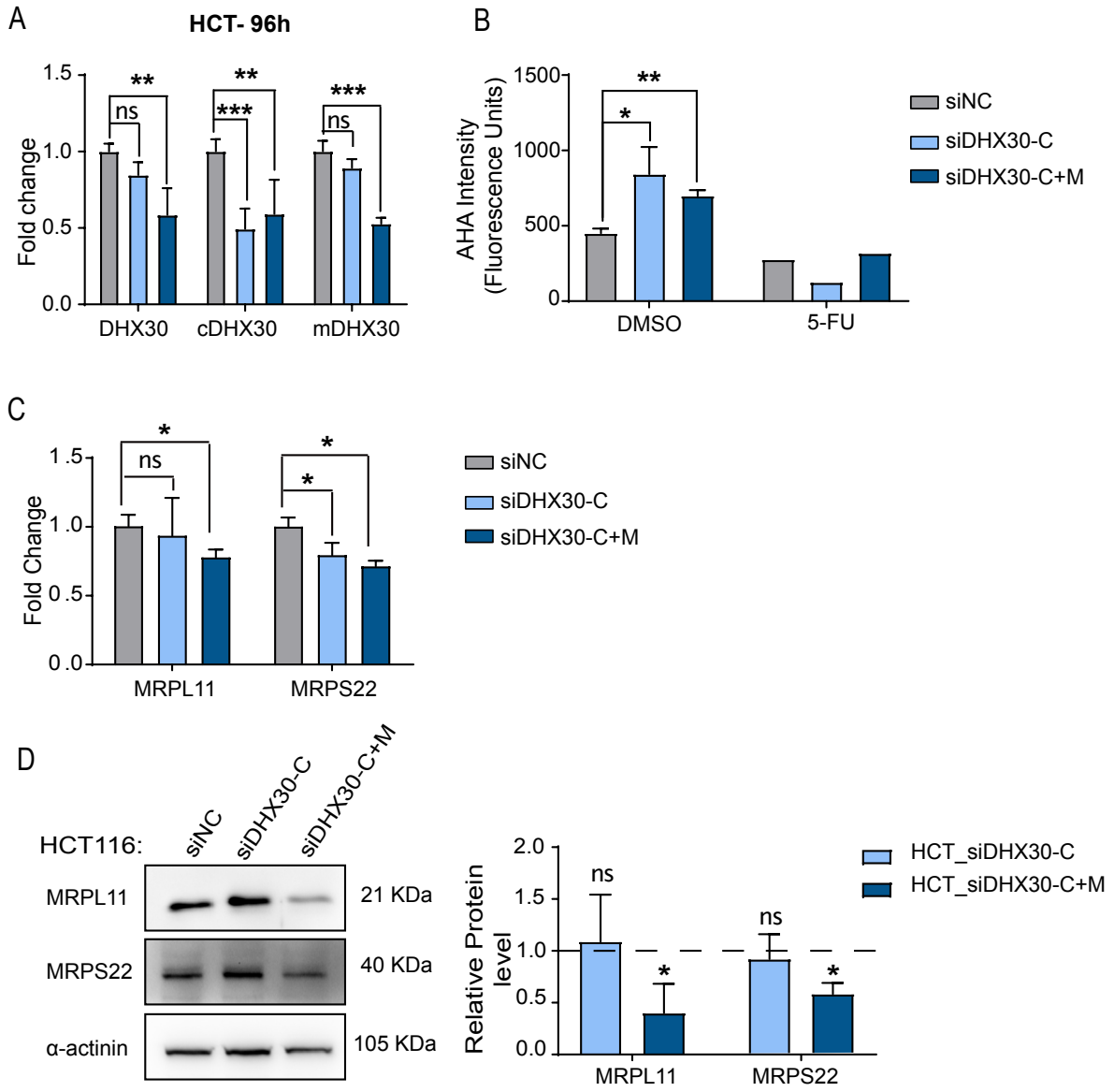

922

923 Figure 4

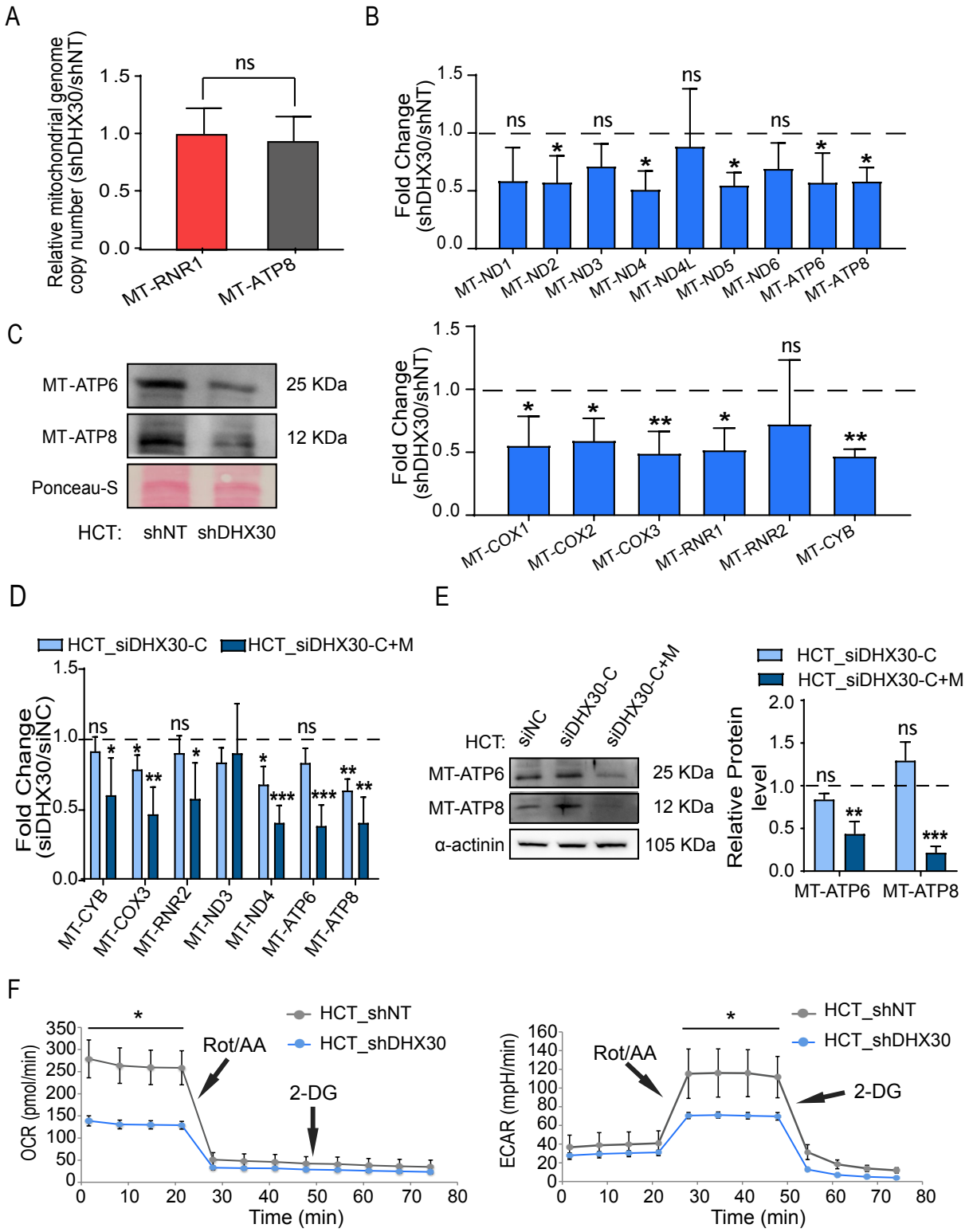

924

925 Figure 5

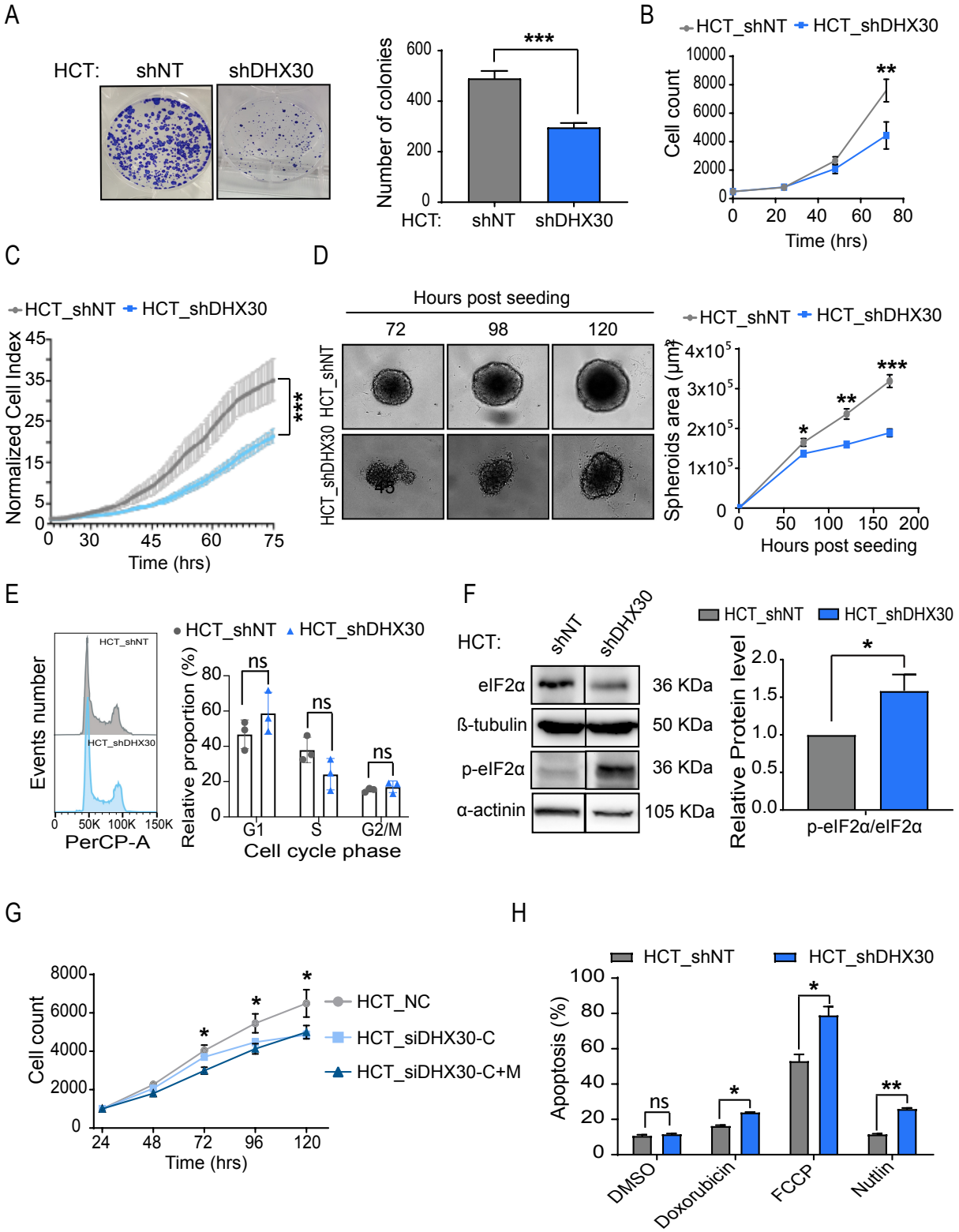

926

927

928 Figure 6

		Data extracted from the GEPIA2 web server^						
		Expression Correlation*		Outcome				
clustering	**tumor type**	R	p-value	HR (high)	Logrank p value	p(HR)	n	**tumor type name**
Cluster1	LAML	0.5	3.10E-12	**2.4**	**0.016**	**0.02**	54	Acute Myeloid Leukemia
	KIRC	0.39	0	**0.69**	**0.017**	**0.017**	516	Kidney renal clear cell carcinoma
	KIRP	0.44	8.90E-15	0.87	0.65	0.65	282	Kidney renal papillary cell carcinoma
	LIHC	0.49	0	**1.9**	**0.00027**	**0.00035**	364	Liver hepatocellular carcinoma
	PRAD	0.44	0	***2.1***	***0.00063***	***0.00083***	492	Prostate adenocarcinoma
	UCEC	0.4	5.70E-11	0.64	0.21	0.22	172	Uterine Corpus Endometrial Carcinoma
	LGG	0.42	0	**1.7**	**0.0045**	**0.005**	514	Brain Lower Grade Glioma
	PCPG	0.52	3.60E-14	*1.2*	*0.74*	*0.74*	182	Pheochromocytoma and Paraganglioma
	THCA	0.59	0	*0.66*	*0.16*	*0.16*	510	Thyroid carcinoma
	ACC	0.67	2.40E-11	**3.3**	**0.0035**	**0.0055**	*76*	Adrenocortical carcinoma
	KICH	0.66	1.70E-09	**9.5**	**0.0096**	**0.0034**	64	Kidney Chromophobe
Cluster 2	DLBC	0.37	1.00E-02	0.65	0.56	0.56	46	Lymphoid Neoplasm Diffuse Large B-cell Lymphoma
	THYM	0.21	2.20E-02	*1.5*	*0.37*	*0.37*	119	Thymoma
	GBM	0.13	9.30E-02	0.98	0.86	0.9	162	Glioblastoma multiforme
	UVM	0.04	7.30E-01	**3**	**0.025**	**0.033**	78	Uveal Melanoma
	PAAD	0.41	1.70E-08	1.3	0.21	0.22	178	Pancreatic adenocarcinoma
	ESCA	0.31	2.30E-05	1	0.99	1	182	Esophageal carcinoma
	SKCM	0.44	0.00E+00	**1.4**	**0.027**	**0.028**	458	Skin Cutaneous Melanoma
	OV	0.17	3.70E-04	0.85	0.18	0.19	424	Ovarian serous cystadenocarcinoma
	STAD	0.35	3.00E-13	0.82	0.21	0.22	384	Stomach adenocarcinoma
	CESC	0.21	3.10E-04	1.1	0.75	0.75	292	Cervical squamous cell carcinoma and endocervical adenocarcinoma
	BLCA	0.31	2.80E-10	1.1	0.63	0.63	402	Bladder Urothelial Carcinoma
	HNSC	0.22	2.70E-07	1.1	0.32	0.33	518	Head and Neck squamous cell carcinoma
	COAD	0.17	4.90E-03	0.79	0.33	0.34	270	Colon adenocarcinoma
	READ	0.37	2.80E-04	0.74	0.53	0.53	92	Rectum adenocarcinoma
	BRCA	0.22	1.70E-13	1.3	0.13	0.13	1070	Breast invasive carcinoma
	LUAD	0.16	6.10E-04	**1.6**	**0.0027**	**0.003**	478	Lung adenocarcinoma
	LUSC	0.2	6.80E-06	0.86	0.27	0.27	482	Lung squamous cell carcinoma
	TGCT	0.17	5.40E-02	*1.4*	*0.34*	*0.34*	136	Testicular Germ Cell Tumors
	CHOL	-0.16	3.70E-01	1.1	0.79	0.8	36	Cholangio carcinoma
	MESO	0.05	6.60E-01	1.5	0.097	0.098	82	Mesothelioma
	SARC	0.12	6.20E-02	1.3	0.25	0.25	262	Sarcoma
	UCS	0.03	8.50E-01	1.2	0.54	0.53	56	Uterine Carcinosarcoma

^ http://gepia2.cancer-pku.cn/#index

* between DXH30 and 14 mitoribosomal transcripts that are derived from the intersection of Translation Efficiency data, Leading Edge in significant terms in GSEA and DH30 eCLIP data in ENCODE: MRPL1, MRPL12, MRPL3, MRPL30, MRPL35, MRPL37, MRPL4, MRPL41, MRPL49, MRPL51, MRPS15, MRPS24, MRPS22, MRPL11

n refers to the total number of samples. These were split at median for the K-M analysis.
Number in italics indicate the DFS instead of OS data was used.

ACC

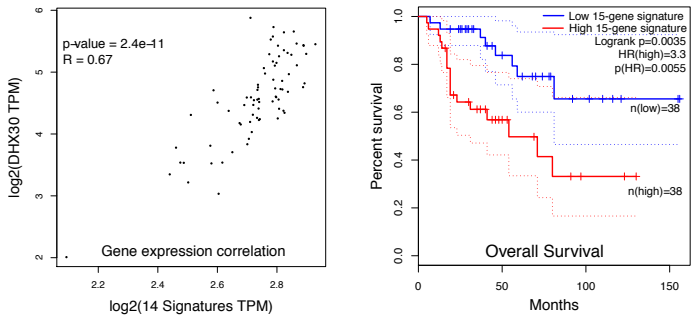

LIHC

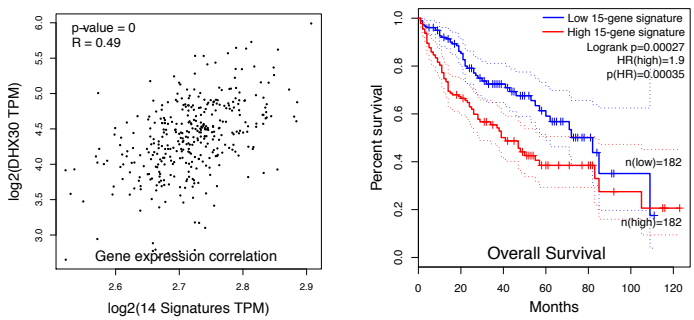

929